Development of Real-Time Particulate and Toxic-Gas Sensors for Firefighter Health and Safety

Final Report

Grant No. EMW-2014-FP-00688

Prepared by

Fumiaki Takahashi, PhD

Department of Mechanical and Aerospace Engineering
Case Western Reserve University
Cleveland, OH 44106
fxt13@case.edu

July 2019

PROJECT DESCRIPTION

This work was performed under a grant from the U.S. Department of Homeland Security, Federal Emergency Management Agency, Assistance to Firefighters Grant Program, Fire Prevention and Safety Grant (No. EMW-2014-FP-00688), following a preliminary study grant (EMW-2012-FP-01284), awarded to Case Western Reserve University.

Research Team

Case Western Reserve University (OH)
- Dr. Fumiaki Takahashi (Principal Investigator)
- Dr. Chung Chiun Liu
- Laurie Dudik

NASA Glenn Research Center (OH)
- Paul S. Greenberg
- Dr. Gary W. Hunter
- Dr. Michael, J. Kulis
- Gordon M. Berger
- Dr. Jennifer C. Xu

Makel Engineering, Inc. (CA)
- Dr. Susana Carranza
- Jeff Williams
- Dr. Darby B. Makel

Project Partners

Fire Protection Research Foundation (MA)
- Casey C. Grant
- Dr. Sreenivasan Ranganathan

USDA Forest Service (ID)
- George Broyles

Cleveland Division of Fire (OH)
- Batt. Chief Sean DeCrane (retired)
- Batt. Chief Thomas Schloemer

Tualatin Valley Fire & Rescue (OR)
- Capt. Patrick Fale

Project Technical Panel

- Bob Athanas, Chair NFPA TC on Electronic Safety Equipment, FDNY (NY)
- Dr. Christina Baxter, DOD / TSWG (VA)
- Nelson Bryner, NIST (MD)
- Robert Doke, Oklahoma State Fire Marshal (OK)
- Martin Harper, NIOSH (WV)
- Max Kiefer, NIOSH (CO), Alternative to M. Harper
- Dave Trebisacci, Staff Liaison, NFPA TC on Electronic Safety Equipment (MA)
- Doug Wolfe, IAB Rep and Sarasota County Fire Rescue (FL)
- Dr. Kenny Fent, CDC/NIOSH/DSHEFS (OH)

TABLE OF CONTENTS

		Page
PROJECT DESCRIPTION		ii
TABLE OF CONTENTS		iii
ABSTRACT		1
1. INTRODUCTION		2
2. BACKGROUND		2
	2.1 Firefighter Exposure	2
	2.2 Health Effects	3
	2.3 Published Exposure Standards	4
3. PARTICULATE SENSOR		4
4. CHEMICAL SENSORS FOR ACROLEIN AND FORMALDEHYDE IN AIR		9
	4.1 Introduction	9
	4.2 Development of Acrolein Gas Sensor	11
	4.3 Membrane-electrolyte formation of the sensor prototype	12
	4.4 Experimental evaluation of the acrolein gas sensor prototype	12
	4.5 Development of Formaldehyde Gas Sensor	15
	4.6 Fabrication of the formaldehyde gas sensor using thin film technology	20
	4.7 Thick film printing of Ag/AgCl reference electrode	23
5. SIC BASED SCHOTTKY DIODE GAS SENSORS FOR DETECTION OF METHANE, FORMALDEHYDE AND ACROLEIN		24
	5.1 Sensor Fabrication	24
	5.2 Testing System	26
	5.3 Test Results	27
6. SYSTEM INTEGRATION		29
	6.1 Introduction	29
	6.2 Prototype I	29
	6.3 Prototype II	38
7. SMOKE CHARACTERIZATION		48
	7.1 Preliminary Study	48
	7.2 Laboratory Experiments	56
	7.3 Field Fire Experiments	59
	7.4 Future Plan	60
8. SUMMARY		60
ACKNOWLEDGEMENTS		60
PUBLICATIONS AND PRESENTATIONS		61
THESES		62
REFERENCES		63

ABSTRACT

A technical endeavor has been made to develop prototypes of real-time particulate and toxic-gas sensors for firefighter health and safety in collaboration between Case Western Reserve University (CWRU), NASA Glenn Research Center, and Makel Engineering Inc. (MEI). Removal of respiratory protection during post-fire overhaul activities can expose firefighters to unknown toxicants, but current practice generally relies on the carbon monoxide detection. Wildland firefighters do not wear respiratory protection despite long-term exposure to smoke at varying levels. Various consecutive and partially overlapping tasks have been conducted.

In the early stage of the project, the Project Technical Panel was formed with the assistance of the Fire Protection Research Foundation, and telephone conferences were held to review the project scope, tasks, timetable, and other pertinent project details.

Two types of micro-fabricated sensors for sensory irritant gases, i.e., acrolein and formaldehyde, were studied at CWRU and NASA. In the meantime, miniaturization of the existing multi-parameter aerosol scattering sensor was completed at NASA. The particulate and gas sensors, together with the control electronics, were integrated into prototypes at MEI. Prototype I units include the sensors for particulate, low-level CO, O_2, and hydrocarbon sensors, and Prototype II units include those for particulate, high-level CO, O_2, hydrocarbon, acrolein, and formaldehyde.

The smoke generation and toxicity characteristics of pyrolizing or flaming materials were studied using the smoke density chamber and the cone calorimeter at CWRU. In addition, a brief attempt was made to test a prototype unit in the wildland fire in California by the USDA Forest Service. Further field fire testing is needed for commercializing a product in the future.

1. INTRODUCTION

An NFPA report [Fahy et al., 2018] shows that approximately 100 firefighters are killed each year while on duty and tens of thousands are injured. Since 1977, the number of U.S. firefighter deaths annually at structure fires has dropped almost two thirds, as the annual number of structure fires declined by 53 % [Fahy, 2010]. Over half of the fatalities are from line-of-duty sudden cardiac events with the others being from traumatic injuries. While the rate of sudden cardiac deaths at structure fires has been dropping, the rate of deaths inside structures due to traumatic injuries, including smoke inhalation or asphyxiation, burns or crushing, has shown marked increases.

There are high-priority needs [Anon. 2011, Anon. 2013] for improvements in personal protective equipment (PPE) and environmental monitoring system to reduce incidence of firefighter exposure of chemicals and particulates during structure fire overhaul activities and in all aspects of wildland fire. The post-fire environmental monitoring system would determine when it is safe to remove respiratory protection. The challenge is to integrate and adapt the technologies effectively and reliably to make the firefighter aware of dangerous situation in their work environment.

Although commercial technologies for particulates and various toxic gases exist on the market, none of these devices measure particulate and gas concentrations simultaneously. Many of them are often too bulky, heavy, and expensive to be incorporated into the integrated package required for this application. The purpose of this project is to develop prototypes of real-time particulate and toxic-gas sensors for firefighter health and safety. Applications of the technology include both structure and wildland firefighting.

2. BACKGROUND

2.1 Firefighter Exposure

Fire smoke is a mixture of liquid and solid aerosols, vapors, and gases that are produced by thermal decomposition (or pyrolysis), smoldering, and combustion of materials. The type and amount of particulates and chemicals in smoke vary, depending on what are burning, how much oxygen (O_2) is available, and the reaction temperature. Contemporary structure firefighting environments contain a variety of toxicants due to synthetic materials and chemicals (e.g., plastics, fabrics, flame retardants, and wood preservatives). Furthermore, toxic chemicals, including those known to be carcinogens, may be absorbed in condensed phase of aerosols.

Fire overhaul is the firefighting stage in which fire suppression is complete and firefighters are searching the structure for hidden fire or hot embers [Bolstad-Johnson et al., 2000; Grant, 2007; Bryant et al., 2007]. The overhaul phase of a fire lasts an average of 30 minutes. During the overhaul phase of a structure fire, when there is little or no smoke in the environment, firefighters are most likely to remove their respiratory facepiece and work in this environment without respiratory protection. Even if no smoke is visible, the environment may still be dangerous. Removal of respiratory protection could expose firefighters and investigators to a variety of toxic gases, vapors, and airborne particulates. Traditionally, firefighters rely upon CO to determine the course of this action [Weiss and Miller, 2011].

A groundbreaking work [Bolstad-Johnson, et al., 2000] on firefighter exposure revealed that during fire overhaul in 25 fires, acrolein (C_3H_4O), CO, formaldehyde (CH_2O), glutaraldehyde ($C_5H_8O_2$) exceeded published ceiling values, and benzene (C_6H_6), nitrogen dioxide (NO_2), and sulfur dioxide (SO_2), exceeded published short-term exposure limit (STEL). Weiss and Miller [Weiss and Miller, 2011] measured toxicant concentrations during overhaul in 38 fires and reported that NO_2, acrolein, CO, arsenic (As) and mercury (Hg) exceeded National Institute for Occupational Safety and Health (NIOSH) Immediately Dangerous to Life and Health (IDLH) levels; glutaraldehyde, hydrogen chloride (HCl), hydrogen cyanide (HCN), ozone (O_3), particulates (<10 μm), and benzene (in addition to the above) exceeded NIOSH Recommended Exposure Level – Short Term (REL – ST) or Occupational Safety and Health Administration (OSHA) Permissible Exposure Limit (PEL). Therefore, these species and particulates are in the most dangerous toxicant groups, next to CO.

On the other hand, many studies on smoke exposure and the resulting adverse health effects among wildland firefighters have long been performed by the US Forest Service [Reinhardt, 1991; Reinhardt and Ottmar, 2004]. Wildland firefighters do not presently wear respiratory protection. Exposure to wildland smoke may be one of the least understood risks of wildland firefighting. Wildland firefighters can be exposed to significant levels of CO and respiratory irritants, including formaldehyde, acrolein, and respirable particulate matter [Reinhardt, T.E., Ottmar, 2004]. Correlations among the pollutants are recommended to be used to predict exposure to several pollutants when resources allow only one (such as CO) to be monitored.

2.2 Health Effects

Numerous studies have demonstrated adverse health effects associated with the respiratory uptake of airborne particles. These studies address both animal and human subjects, and span controlled laboratory exposure and actual conditions encountered in the field. With improved understanding, distinctions have emerged regarding deposition mechanisms pertaining to different size regimes, spanning coarse (> 1 μm) to ultrafine (< 100 nm) particles. Epidemiological studies have consistently shown an association between particulate exposure, exacerbating existing respiratory illnesses, and also increased rates of cardiovascular and respiratory diseases [Seaton, 1995; Laden et al., 2006; Pope and Dockery, 2006; Peters et al., 2001; Gold et al., 2005; Ibald-Mulli et al., 2004].

In particular, elevated rates of coronary disease and morbidity are observed in firefighters engaged in suppression and overhaul activities [Kales et al., 2005; Geibe et al., 2008; Burgess et al., 2001; Holder et al., 2006]. These occurrences have been associated with exposure to particulates [Baxter et al., 2010], and are consistent with other clinical studies examining particle exposure in workplace environments [Gong et al., 2008; Samet et al., 2009; Torén et al., 2007]. Adverse respiratory effects have been associated with Firefighters engaged in overhaul [Burgess et al., 2001], and measurements of wood smoke particles in wildland fires have demonstrated as a mechanism for cellular injuries [Leonard et al., 2000]. Data from a wide variety of suppression and overhaul scenarios consistently confirms the presence of particulates known to constitute a hazard to human respiratory health [Geibe et al., 2008].

International Association of Fire Fighters (IAFF) launched an educational campaign called “The Silent Killer” [Cumpston and Rose, 2017]. to emphasize the hazards of occupational exposure to carbon monoxide (CO) and to reduce the known risk factors that can kill or injure firefighters

[Hall and Schnepp, 2011]. It has been known that there exists a role of the other "toxic twin" in fire smoke, i.e., cyanide (CN-), in the acute toxicity of smoke inhalation and its probable role in LODDs and sudden cardiac illness. As a result of increased use of polymeric materials, the risk of CN- poisoning has increased [Alarie, 1985; Stefanidou and Athanaselis, 2004; Bowes, 1974]. There are numerous papers available in the literature on fire smoke inhalation and toxicology [Bauer and Ginbel, 2004; Birky and Clarke, 1981; Jones et al., 1987; Jones and Krohmer, 1990; Yoshida et al., 1991; Yeoh and Braitberg, 2004; Alarie, 2002; Stefanidou and Athanaselis, 2004; Hartzell, 1996; Lowry et al., 1985; Pryor et al., 1975; Norris et al., 1986] and concentration measurements of smoke and toxic gases encountered by firefighters [Jankovic et al., 1991; Brandt-Raul et al., 1988; Gold et al., 1978; Breen et al., 1995; Treitman et al., 1980].

2.3 Published Exposure Standards

The type of toxicants to be monitored should be selected from the species which exceeded the published exposure standards in the field measurements [Bolstad-Johnson, et al., 2000; Weiss and Miller, 2011; Reinhardt, T.E., Ottmar, 2004]. The range of measurement for each species must be based on the standard exposure limits. Table 1 shows the published exposure standards [Anon., 2014; Anon., 2006; Kulis et al., 2014] for selected toxicants of interest. A CO level of below 35 ppm (NIOSH REL) has traditionally been the acceptable limit for firefighters to doff their self-contained breathing apparatus (SCBA) and wear lesser level of respiratory protection [Weiss and Miller, 2011]. The sensors must have sufficient accuracy and precision to measure the levels of the lower exposure limits (OSHA PEL ACGIH TLV, and NIOSH REL).

3. PARTICULATE SENSOR

The particulate sensor included in the integrated package is based on a design previously developed at the NASA-Glenn Research Center. This device is called an MPASS: Multi Parameter Aerosol Scattering Sensor. The MPASS employs multi-angle light scattering to determine aerosol properties.

The present embodiment consists of three photodetectors located at fixed angular locations. These angles are specified relative to a focused, monochromatic laser source. All of the components used to construct this sensor are traceable to mass market technologies such as CD/DVD drives, supermarket scanners, laser pointers, etc. This provides numerous desirable features such as low cost, low power consumption, mechanical resilience, and high reliability. The associated components used to assemble this sensor are shown in Figure 1. The opto-electronic assembly is housed in a compact, 50 mm square by 1 cm thick package as seen in Figure 2. The external housing was 3D printed to conform to the overall goal of providing sensors capable of being produced at a low cost point for end users. The MPASS is designed as a passive sampling device, wherein ambient aerosols can readily pass through a 1 cm diameter central passage. For the present application, the MPASS is located internally to the complete multi-sensor package, so a miniature blower is used for active sampling. This blower is a similar, low cost, high reliability component developed for cooling handheld electronic devices, providing a 10,000+ hour lifetime with milliwatt power consumption.

Table 1. Exposure Standards of Selected Toxicants

Chemical	Formula	OSHA[a] PEL[b]	ACGIH[c] TLV[d]	NIOSH[e] REL[f]	STEL[g]	IDLH[h]
Acrolein	C_3H_4O	0.1 ppm	0.1 ppm	0.1 ppm	0.1 ppm (C[i])[c] 0.3 ppm[e]	2 ppm
Benzene	C_6H_6	1 ppm	0.5 ppm	0.1 ppm	5 ppm[a] 2.5 ppm[c] 1 ppm[e]	500 ppm
Carbon monoxide	CO	50 ppm	25 ppm	35 ppm	200 ppm (C[i])[e]	1200 ppm
Formaldehyde	CH_2O	0.75 ppm	0.3 ppm	0.016 ppm	2 ppm[a] 0.3 ppm (C[i])[c] 0.1 ppm (C[i])[e]	20 ppm
Glutaraldehyde	$C_5H_8O_2$	none	0.05 ppm	0.2 ppm	0.05 ppm (C[i])[c] 0.2 ppm (C[i])[e]	N.D.
Hydrogen chloride	HCl	5 ppm	none	5 ppm	2 ppm (C[i])[c] 5 ppm (C[i])[a,e]	50 ppm
Hydrogen cyanide	HCN	10 ppm	10 ppm	4.7 ppm	4.7 ppm (C[i])[c]	50 ppm
Nitrogen dioxide	NO_2	5 ppm	3 ppm	1 ppm	1 ppm[e] 5 ppm[c] 5 ppm (C[i])[a]	20 ppm
Ozone	O_3	0.1 ppm	0.05ppm[j] 0.08 ppm[k] 0.1 ppm[l] 0.2 ppm[m]	0.1 ppm	0.1 ppm (C[i])[e]	5 ppm
Particulates, respirable	---	5 mg/m^3	3 mg/m^3	---	---	---
Particulates, total	---	15 mg/m^3	10 mg/m^3	---	---	---
Sulfur dioxide	SO_2	5 ppm	2 ppm	2 ppm	5 ppm[c, e]	100 ppm

[a] Occupational Safety and Health Administration (OSHA).
[b] Permissible exposure limit.
[c] American Conference of Governmental Industrial Hygienists (ACGIH).
[d] Threshold limit value.
[e] National Institute for Occupational Safety and Health (NIOSH).
[f] Recommended exposure limit.
[g] Short-term exposure limit.
[h] Immediately dangerous to life or health.
[i] Ceiling (not to be exceeded).
[j] Heavy work.
[k] Moderate work.
[l] Light work.
[m] Heavy, moderate, or light work (≤2 hours).

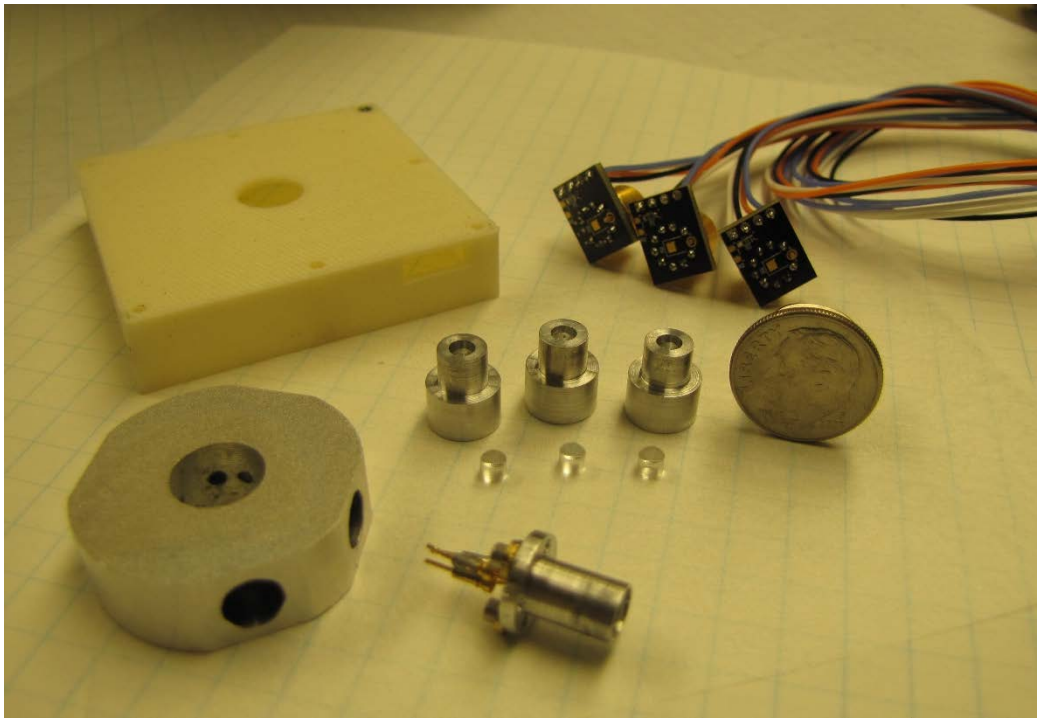

Figure 1. Internal components of the MPASS sensor.

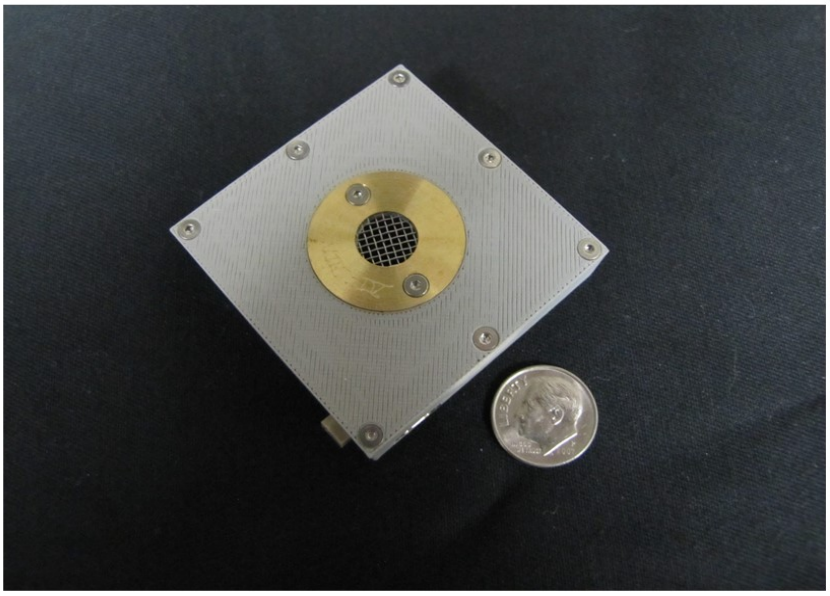

Figure 2. Complete MPASS sensor package.

While novel in terms of size, weight, and power consumption, the most significant feature of the MPASS is the underlying data analysis algorithm. The limitation of existing devices arises from the fact that differing types (size and composition) of particles scatter light differently. This situation is best illustrated by example.

Generally, the requirement is to measure what are referred to as moments of the aerosol. Moments express properties such as the total number of particles per volume (0^{th} moment), their total surface area (2^{nd} moment), or most commonly their total mass (3^{rd} moment). Consider the case where we fix the total mass, but allow the size or composition of the particles to vary. We observe that the scattered light varies considerably among the family of aerosols all having the same total mass. To date, the only way to handle this situation is to calibrate the sensor using exactly the type of particles that ultimately will be measured in the field. If the particles we encounter are different, the calibration will be invalid. This limitation is referred to as a lack of extensibility, and is hugely important in practice. In a firefighting environment, it is impossible to know in advance precisely what combination of materials and conditions (and therefore particles) will be encountered.

The proprietary algorithm used in the MPASS affords the ability to optimize the measurement accuracy based on estimates of the types of particles that will be encountered. Considerable research has been conducted on particles produced in the firefighting environment, and this information is used to establish estimates on what particles will actually be present. In this setting, the anticipated ranges of particle properties are supplied as inputs to the MPASS analysis algorithm. The algorithm then calculates the angularly dependent light scattering arising from all possible combinations of particle properties within these ranges. This information is used to calculate the optimal way to mathematically utilize the multi-angle detector data to obtain measurements of the desired moment.

Figure 3 provides a graphic illustration of this process. One axis is the Count Median Diameter (CMD), conveying the size of the particles. The second axis is $Sigma_g$, which is a measure of the width of the particle size distribution. This single plot corresponds to a refractive index of 1.51, which is typical of combustion generated aerosols. However, the actual algorithm considers a range of refractive indices corresponding to all particle types likely to be present.

Having optimized the measurement for these anticipate ranges, this plot shows how the resulting errors are distributed. The most relevant feature is the median error shown in the upper left hand corner. This conveys that on average, the measured 3^{rd} moment (total mass) for any particle within these ranges will be within 17% of the true value. The measurement optimization is done in post processing, and because the raw data from each detector is saved, the result can be re-optimized after the fact if additional information on the particle properties can be made available. User tools are also available to tailor the resulting plot for differing applications, e.g. if it is desirable for example to emphasize the measurement accuracy of smaller sizes or a band of sizes at the expense of the accuracy in other regions.

The significance of this approach can be seen in rather dramatic terms in Figure 4. The data corresponds to actual field conditions, and was acquired in a firefighting training facility. The materials consist of straw bales, wooden pallets, and articles of furniture, and are combusted inside a purpose-built confined structure. Towards the end of each trial, the fires are extinguished with water using the same hoses and nozzle systems as in the field. The MPASS

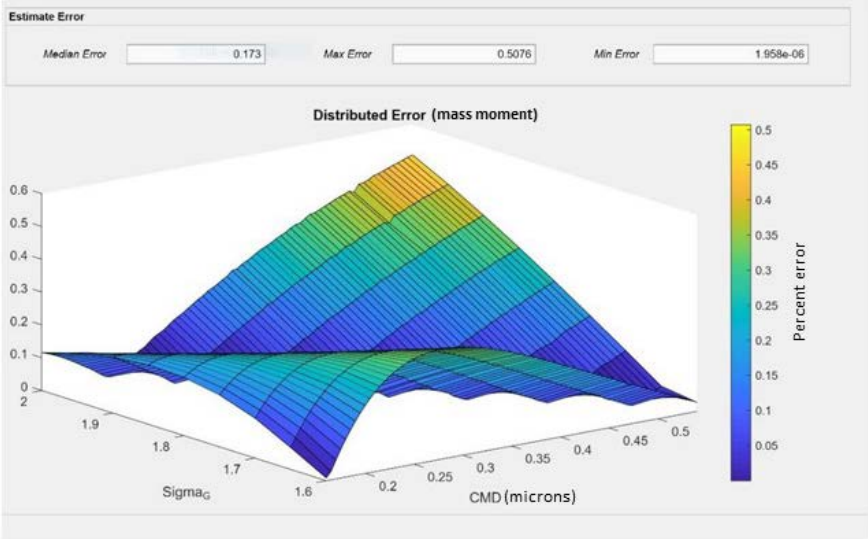

Figure 3. Typical distributed error plot for optimized measurement configuration.

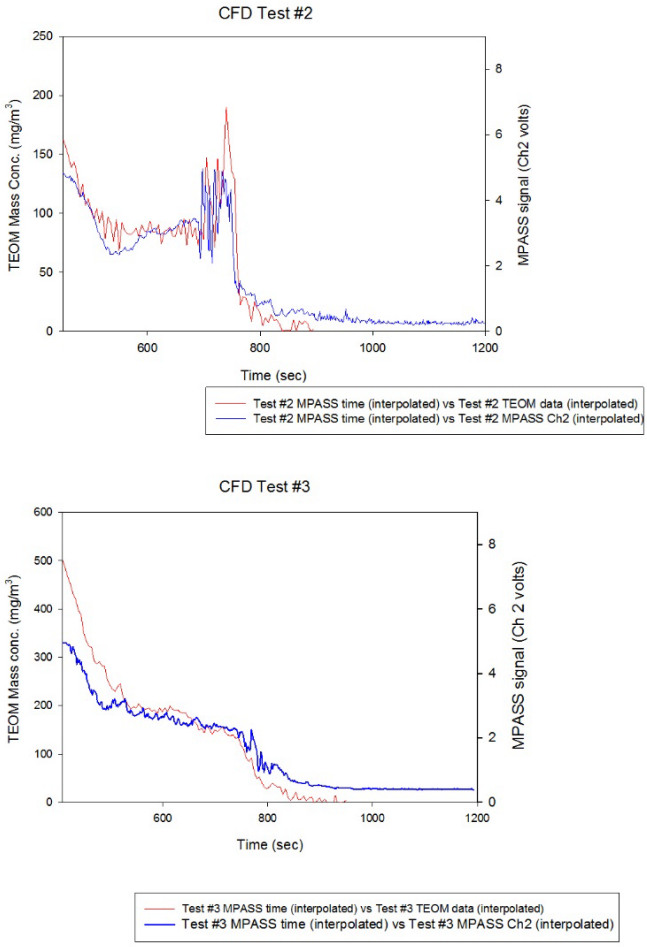

Figure 4. Actual combustion data demonstrating comparison of MPASS and TEOM.

was used to measure the total mass, and the plots show this data compared with a reference, direct-reading mass instrument (a Tapered Element Oscillating Microbalance, or TEOM). Although the size and composition of the aerosol is constantly changing throughout each test, the MPASS can be seen to accurately track the true mass being produced.

At this stage of development, the MPASS has evolved into a product of potential commercially viability. This results from a focused effort to provide a sensor with unique and useful capabilities, combined with attributes of small size and mass, durability, and low cost. As used in this project, functions such as data logging and analysis are handled by a central processor that accommodates the multiple gas-phase sensors as well. A stand-alone version of the MPASS has also been developed, and contains all these same functions internal to the package. A PC based, user friendly graphical interface access allows the sensor to be programmed and calibrated, and includes self-diagnostics, data retrieval, and display. A version is presently being designed to communicate wirelessly with smart devices, and store data remotely on the cloud. More information on these cap[abilities can be accessed through the NASA Glenn Technology Portal at:

https://technology-grc.ndc.nasa.gov/patent/LEW-TOPS-19 and
https://technology.grc.nasa.gov/featurestory/mpass

4. CHEMICAL SENSORS FOR ACROLEIN AND FORMALDEHYDE IN AIR

4.1 Introduction

This task involved the sensor development at the Electronics Design Center (EDC) and the Department of Chemical & Biomolecular Engineering of Case Western Reserve University.

Enhancing the safety of the public and firefighters from fire and related hazards are of critical importance. The primary objective is to reduce injury and prevent death among high-risk populations, particularly for the fire fighters. In order to achieve this goal, early detection of essential gaseous components in the air is necessary. Of many gaseous components in the air for any potential fire hazard, acrolein and formaldehyde are two of the gaseous components should be detected and quantified in a simple effective manner, and chemical sensors are potentially suitable for the applications. The consideration of chemical sensors for the detection of acrolein and formaldehyde will eliminate the use of gas chromatography, spectrometer which require expensive equipment and highly trained operators which will not be practical for fire safety and prevention.

Acrolein is a short-chain vinyl aldehyde which is known to contribute to photochemical smog (early sign of a fire hazard) and irritants of skin and eyes. Level of 4 ppm of acrolein will result to the irritation of eyes and this high concentration limits the detection of acrolein in air for early fire prevention. Traditional analysis and detection of acrolein requires the use of liquid or gas chromatographic techniques which will not be practical for this application. In an early study by the Division of Environmental Planning of Tennessee Valley Authority (TVA), Chattanooga, Tennessee and Office of Research and Development of US Environmental Protection Agency (EPA), Washington, D.C., the detection of acrolein in liquid phase (water or vegetable oil) was attempted using an electrochemical technique and mercury dropping electrode. [Howe, 1976] This study suggested that acrolein can be detectable in liquid phase electrochemically. However, the use of mercury electrode is prohibited today due to the environmental concern of mercury. Also, the advance of electrochemical detection instrument suggests that a better design and

fabrication of both the sensor elements and the measuring instrument can be significantly improved. Specifically, we will use micro-fabrication techniques to design and fabrication the sensor for acrolein detection in air. This development is consistent and compliment the strength and expertise of NASA Glenn Research Center for their "Lick and Stick" leak sensor system technology [Hunter et al., 2010]. This collaboration will be cost-effective and will combine the expertise for this research endeavor.

Thus, an electrochemical based sensor platform was established and developed fabricated by micro-fabrication process for the detection of acrolein and formaldehyde in air in this task. A three-electrode configuration electrochemical sensor was designed and fabricated. Both the working and the counter electrodes were sputtering gold or platinum thin film in the thickness of 50-150 nm. Because the thin film deposition was accomplished at the atomic level, and the resulted film was highly uniform and reproducible. The sensor prototype was constructed on polymeric thin layer substrates providing the flexibility and cost-effective of the substrate itself. The reference electrode was Ag/AgCl [Molazemhosseini et al., 2016]. Reference electrode in general should be highly reversible and this sensor intends to be used in air, the stability of AgCl in air may be a concern. Therefore, a Ni/NiO reference electrode is included in the consideration as a potential reference electrode as an alternative in this study.

The design of this platform sensor is shown in Figure 5

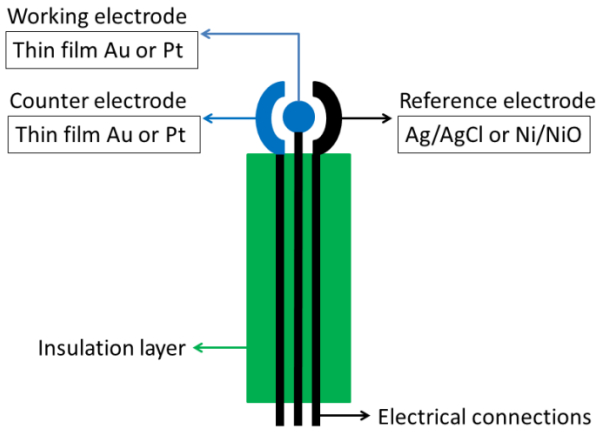

Figure 5. Design of the sensor platform structure.

Cyclic voltammetry (CV) and differential pulse voltammetry (DPV) were used as the electrochemical detection techniques for this study. Cyclic voltammetry identified the applied voltage for the electrochemical reactions for the acrolein in air. DPV was a derivative of linear sweep voltammetry, with a series of applied voltage pulses superimposed on the potential linear sweep steps. Consequently, the current was measured before each potential change, and the current difference was recorded as a function of potential. In this measurement, the effect of the charging current was minimized, and high sensitivity was achieved. Furthermore, Faradaic current was extracted, and the electrochemical reactions was analyzed precisely.

Our research effort in this sub-contract focused on the design, fabrication, preliminary test of the sensor performance and their adoptability into the overall portable sensor microsystem for practical applications in firefighting. Specifically, we devoted our research efforts on the

development of acrolein and formaldehyde gas sensors using electrochemical based technology and micro-fabrication processing.

Acrolein and formaldehyde are two of the many gaseous components found in the air during a fire hazard. They need to be detected and quantified in a simple effective manner and chemical sensors are potentially suitable for this application. The use of chemical sensors for the detection of acrolein and formaldehyde will eliminate the use of gas chromatography which requires expensive equipment and highly trained operators, both of these requirements are not practical for fire safety and prevention in the field.

4.2 Development of Acrolein Gas Sensor

As mentioned, an electrochemical based platform sensor with a three-electrode configuration shown in Figure 1 was designed and fabricated by micro-fabrication process. Specifically, thin gold film was deposited on polyethylene terephthalate (PET) by sputtering technique without any binder and the sensor was patterned by laser ablation technique. Separate masks were used producing different elements of the sensor prototype. The Ag/AgCl reference electrode and the insulation layer were thick-film printed using DuPont #5870 Ag/AgCl and Nazdar APL 34 silicone-free dielectric inks respectively. 100 individual biosensors in 4 rows were fabricated on each PET sheet (355 x 280 mm^2). The overall dimensions of an individual sensor were 33.0 x 8.0 mm^2. The working electrode area was 1.54 mm^2 accommodating 10-15 µL of liquid test sample or gas sample in a flow chamber [Molazemhosseini et al., 2016]. The combination of sputtering and laser ablation techniques resulted in producing a very thin and yet uniform gold layer featuring high-reproduction. The sensor can be manufactured in a roll to roll process making the sensor very cost-effective. Figure 1 shows the platform structure of this sensor prototype, and Figure 6 shows the role-to-role industrial manufacturing process and the dimensions of this acrolein gas sensor:

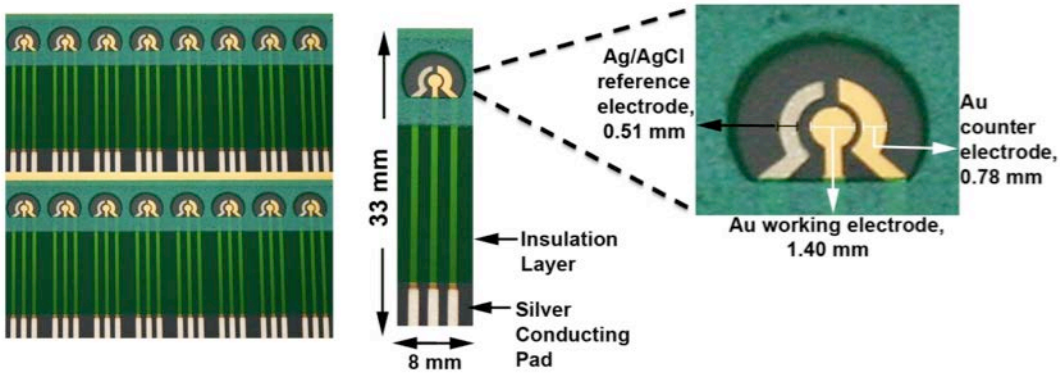

Figure 6. Manufacturing approach, the dimensions and structure of the designed acrolein sensor.

As mentioned, this sensor has been designed and arranged to be manufactured by an external vendor, Conductive Technologies, York, Pennsylvania, demonstrating that this sensor can be produced on large industrial scale and with high degree of uniformity and reproducibility. We have now completed the manufacturing process of the acrolein gas sensor working closely with our vendor.

4.3 Membrane-electrolyte formation of the sensor prototype

This acrolein gas sensor intended to be used in gas phase measurement and without an aqueous electrolyte. Thus, in this study, a membrane-electrolyte was formed allowing the sensor to be operated in solid state without an aqueous solution. Nafion was a Du Pont product. It was a sulfonated tetra-fluoroethylene based fluoropolymer-copolymer. The perfluoro-vinyl ether groups terminate with sulfonate groups gave Nafion of the unique ionic conductivity. Consequently, Nafion had been used as polymeric membrane electrolyte for fuel cell and other electrochemical energy storage systems. Nafion was also known for not conducting anions or electrons. Thus, Nafion was chosen as the basic membrane-electrolyte material for this acrolein gas sensor. Liquion (15% Nafion and 85% alcohol w/w%; Cat No: 1115, Ion Power Inc. New Castle, DE 19720) was chosen and used to provide the Nafion. The conductivity of Nafion was only fair, and in order to enhance the conductivity of the Nafion-based electrolyte, diethylene glycol (Cat. No: 111-46-6, Sigma-Aldrich St. Louis, MO 83103) was considered to be added into the mixture [Swann, 2003] enhancing the conductivity of this Nafion based electrolyte. However, this modification will be attempted based on the preliminary test results. Also, a dilute H_2SO_4 solution, such as 0.1M may be added into the Nafion solution enhancing further about the ionic conductivity of the membrane-electrolyte. Thus, in this modification, we provided a membrane-electrolyte for the acrolein gas sensor allowing it to be operated in solid state.

4.4 Experimental evaluation of the acrolein gas sensor prototype

Figure 7 shows the experimental arrangement of the evaluation and test of the acrolein sensor. Acrolein gas of 10 ppm (parts per million) in N_2 (Airgas Co, La Porte, TX-) was used, diluted and mixed with pure N_2 providing a range of acrolein gas in 5 ppm and lower for the evaluation. A MKS Multi-Gas Controller Model 6471S with two gas inlet channels was used to provide acrolein gas of different ppm levels feeding into the test chamber. Figure 8 shows the structure and dimensions of the test chamber. The test chamber was fabricated with thin plastic, 5 mm in thickness. It was approximately 12.7 cm X 7.6 cm X 6.4 cm (5” X 3” X 2.5”) in size with small valves at both inlet and outlet of the test chamber. The construction material and the exact dimensions of the test chamber were not critical and could be changed or modified, if needed. The testing sensor was connected to a CHI 660 Model A-E Electrochemical Workstation (CH Instrument Model 660 A-E, Austin, TX) The connector was an edge connector (Hirose electrical company FH21-6S-1DS) which was cemented with epoxy on one side-wall of the test chamber. The acrolein gas sensor was then directly connected to the Electrochemical Workstation. The Workstation was connected to a desk-top computer (OptiPlex 3040 Micro PC desktop, Dell, Round Rock, TX). Between runs for testing different levels of acrolein gas, the test chamber was purged with pure N_2 gas. Pure N_2 gas was fed through the Multi-Gas Controller as described above to the test chamber. At this juncture, both the inlet and outlet valves were kept opened. The gas flow rate of N_2 gas was set at 250 cc/minute (CCM), and it usually required three minutes to complete this purge process.

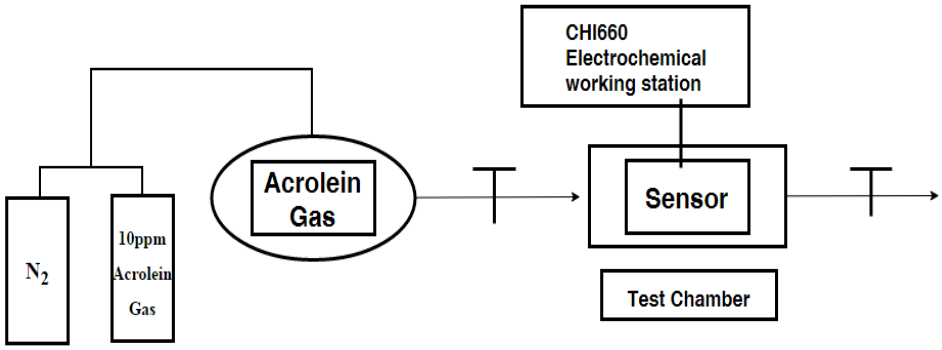

Figure 7. Experimental assembly for testing of acrolein gas sensor.

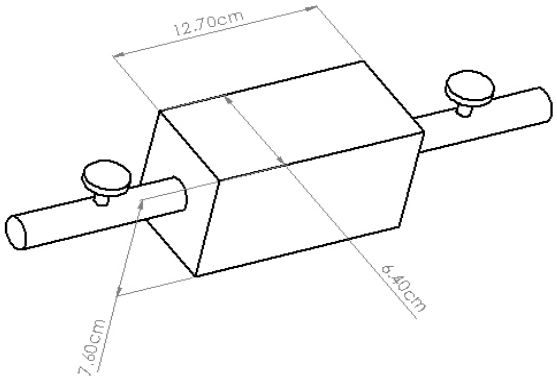

Figure 8. Schematic of the test chamber for the sensor.

Different Pulse Voltammetry (DPV) was used for the electrochemical measurement in this study. Cyclic voltammetry and amperometric voltammetry are commonly used for the measurement immediately. However, DPV is a linear sweep voltammetry with a series of regular voltage pulses superimposed on the linear potential sweep. The current is then measured before each potential change. In this measurement, the effect of the charging current can be minimized, achieving a higher sensitivity. Also, Faradaic current of the electrochemical reaction is extracted, so that the reaction can be analyzed more precisely. Thus, in this study, we aimed to use DPV measurement providing higher sensitivity of the biosensor compared to cyclic voltammetry and amperometric voltammetry. DPV measurement was also used in the earlier study of acrolein gas sensor as reported in "Voltammetric Detection of Acrolein" which was reported by U.S. Environmental Protection Agency, Washington D.C [Howe, 1976].

Figures 9 and 10 shows the typical and acuminated combined test results of this acrolein gas sensor over the concentration range of 0-2.0 ppm in nitrogen.

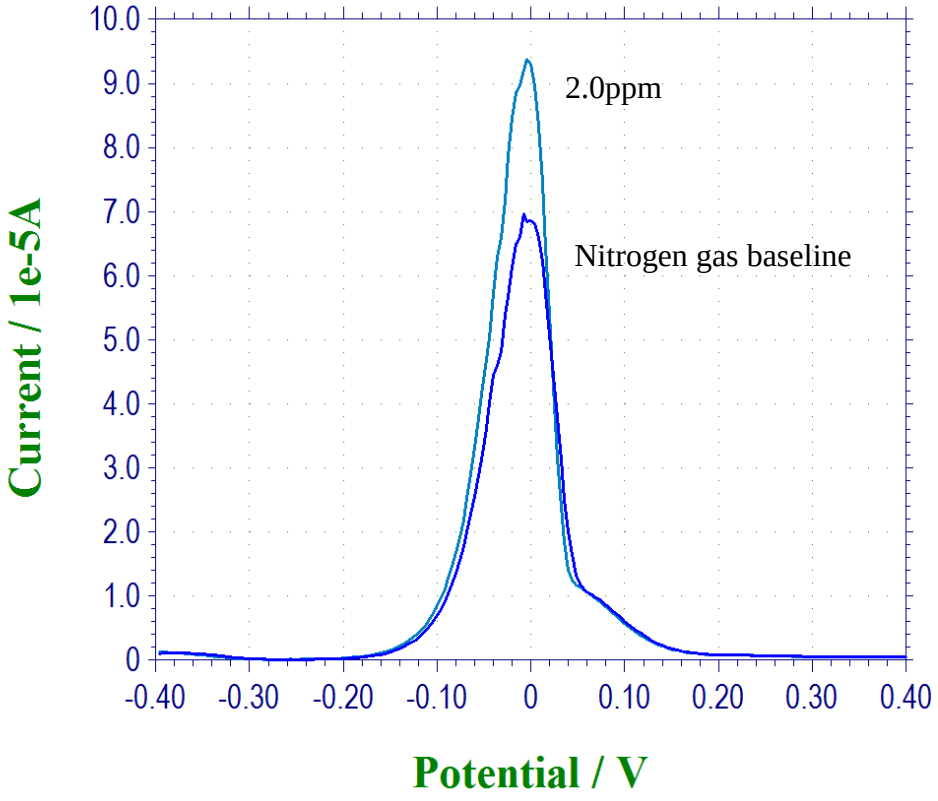

Figure 9. DPV measurements of acrolein gas in nitrogen at acrolein concentration range of 0 and 2.00 ppm.

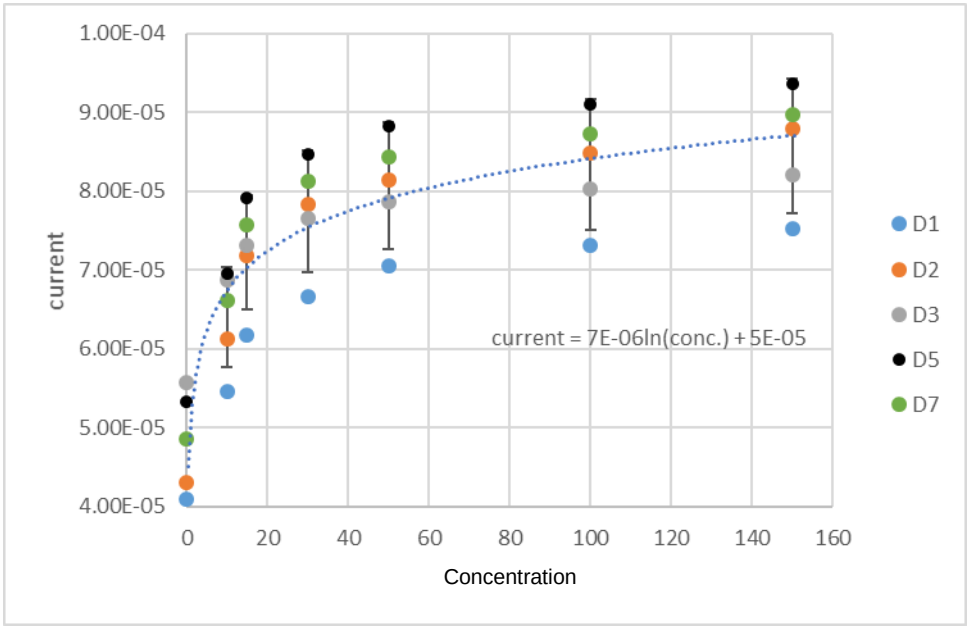

Figure 10. Acuminated combined DPV measurements of acrolein gas in nitrogen over the acrolein gas concentration range of 0-2.00 ppm.

4.5 Development of Formaldehyde Gas Sensor

Formaldehyde is another gaseous component for fire prevention detection and health hazard. Various analytical methods have been described for the determination of formaldehyde vapor. Most common detection technique of formaldehyde in air is by absorption that formaldehyde is absorbed into a solution or a filter. The resulting solution is then analyzed by ion chromatography [Lorrain et al., 1981] or high-performance liquid chromatography [Levin J.O. et all, 1985]. Alternatively, electrochemical methods may be used for the determination of formaldehyde in liquid phase [Chung et al., 2013]. Formaldehyde can be oxidation electrochemically and this approach of detecting formaldehyde has been demonstrated using platinum electrode. [Bagotzky and Vasilyev, 1964] However, continuous exposure of platinum electrode to formaldehyde results in a decrease in sensitivity of the sensor. This is due to the typical electrochemical oxidation of organic compounds on noble metal electrode (or catalyst) leading to a fouling of the electrode. Instead of using platinum as the electrode material, we propose to use iridium as the electrode material instead. This approach is based on results of various investigations including the US Patent by Auel et al. [1987].

In this sub-contract, the Electronics Design Center (EDC) of Case Western Reserve University plan to carry out the design and fabrication of a formaldehyde gas sensor prototype. Because of safety regulation in University, the testing of the formaldehyde gas sensor will be carried out by researchers in NASA and Makel Engineering Inc. The design and fabrication process of this formaldehyde sensor are described and discussed in this section of the Final Technical Report of the sub-contract. Similar to the acrolein gas sensor, a three-electrode configuration electrochemical sensor for the detection of formaldehyde was designed. However, both the working and counter electrodes were sputtered palladium thin film based on the catalytic activity of palladium toward formaldehyde. Different metallic films for the working and counter electrodes including iridium were assessed, and palladium was chosen in this development. The thickness of the palladium will be 1000 Angstroms with a 100 Angstrom layer of titanium underneath of it enhancing the adhesion of the palladium layer to the underlying polymeric substrate. Because thin film deposition was accomplished at the atomic level, the film was highly uniform and reproducible. The reference electrode was thick film (screen) printed Ag/AgCl. The substrate for the sensor will be PET (U.H.M.W. polyethylene). The Ag/AgCl thick film ink was commercially available and was used in this manufacturing process of the formaldehyde gas sensor.

Figure11 illustrates the processing steps in this fabrication process:

(a) Step 1 – PET substrate – Ultra High Molecular Weight Polyethylene 0.2 mm thick.

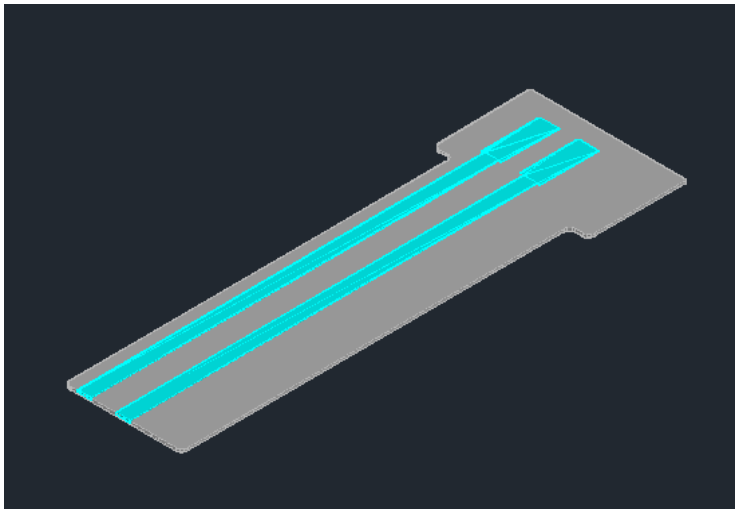

(b) Step 2 – Using lift-off process, pattern the PET substrate and deposit 100 Å titanium/1000 Å palladium using DC magnetron sputtering.

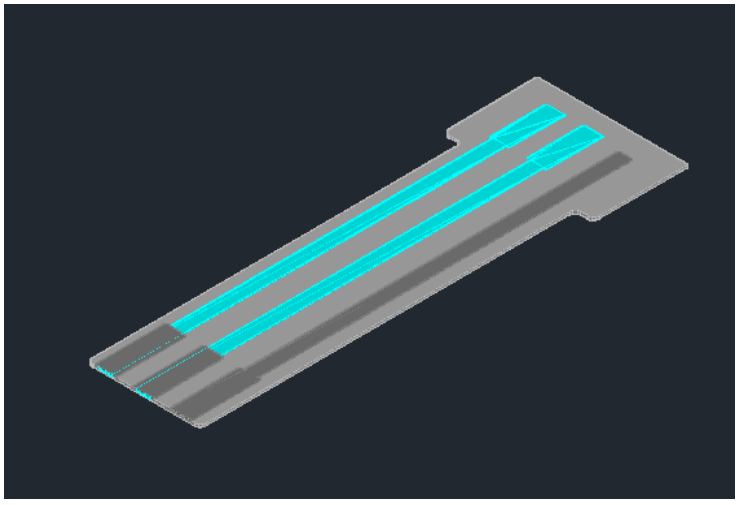

(c) Step 3 – Using thick film (screen) printing deposit a layer of silver over the areas of the palladium electrodes that will be used to connect to the testing equipment. The connector to the

testing equipment is a reusable edge connector. A silver pad and lead is also deposited that will connect to the reference electrode.

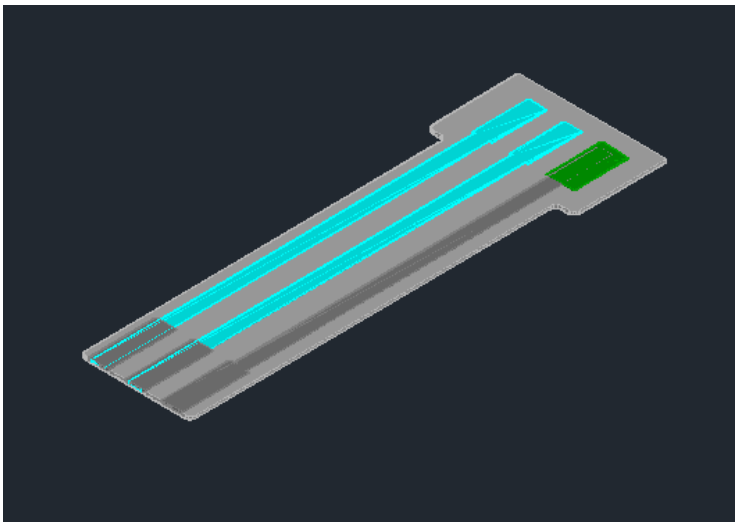

(d) Step 4 – Using thick film (screen) printing deposit the Ag/AgCl reference electrode.

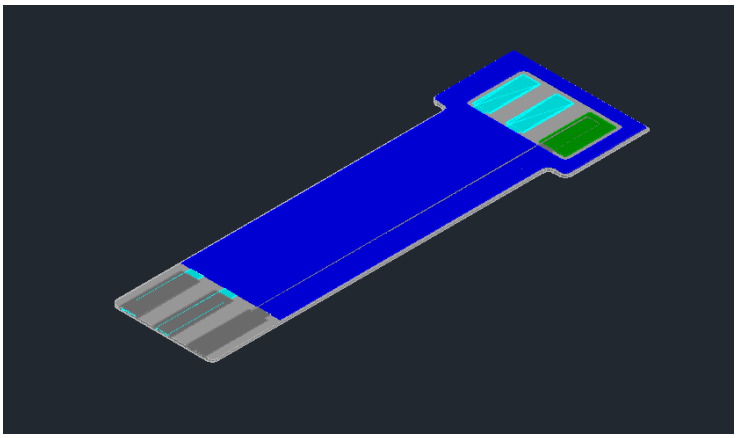

(e) Step 5 – Using thick film (screen) printing deposit a non-conductive insulation area over the palladium and silver leads to prevent shorting and define a well where the solid electrolyte (H2SO4 + Nafion) will be deposited.

Figure 11. The processing steps in this fabrication process.

Based on the steps described above an overview of the final formaldehyde gas sensor can be shown as follow

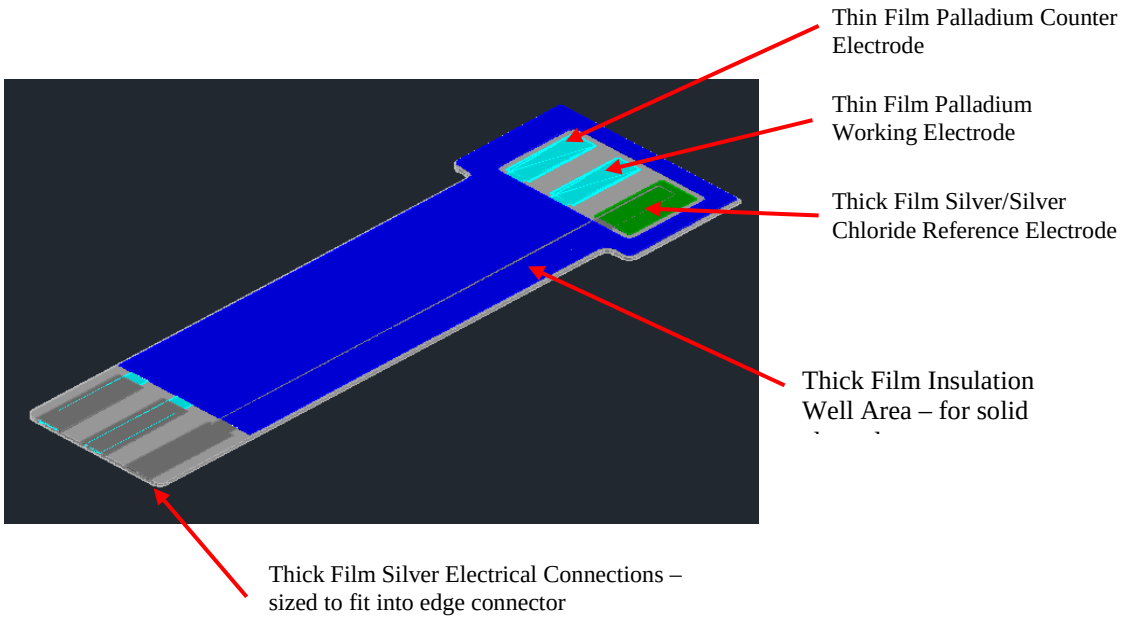

Figure 12. The formaldehyde gas sensor.

We recognized that the size of the working electrode will affect the overall performance of the formaldehyde gas sensor. Therefore, three different designs of the sensor were fabricated and evaluated. Among these three different versions of the formaldehyde gas sensor, the size of the working electrode was varied providing experimental assessment of the performance of the sensor related to its surface area. The overall diameter of the substrate the sensors was 100 mm, therefore there was sufficient space to accommodate several sensor variations.

The overall size of the sensor and the three versions of the sensor are shown in Figure13, and all dimensions are given in millimeters:

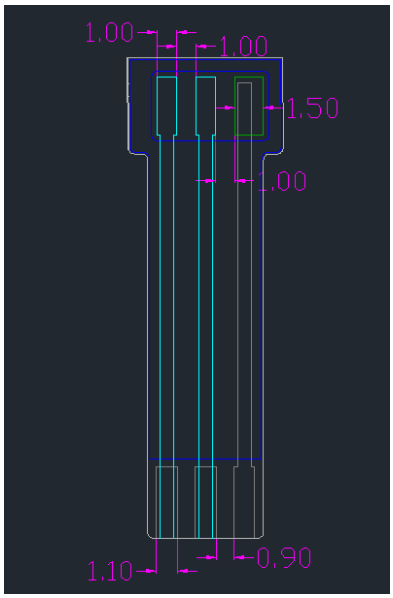

(a) Design 1 – Counter and Working Electrodes Same Size.

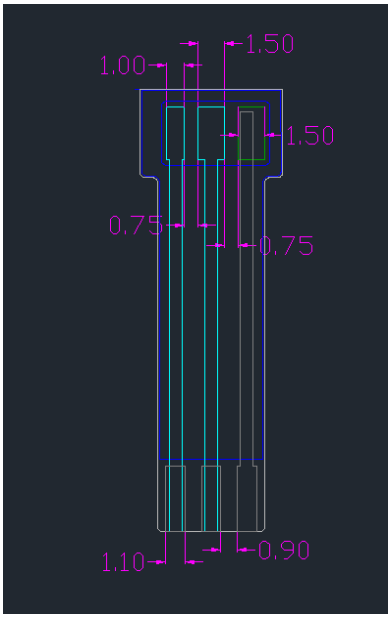

(b) Design 2 –Working Electrode Larger than Counter Electrode.

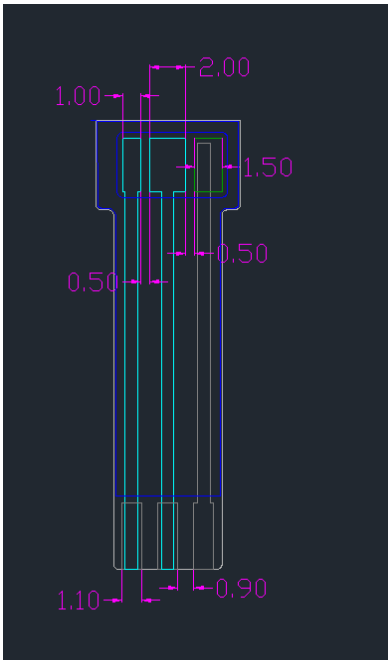

(c) Design 3 –Working Electrode Much Larger than Counter Electrode.

Figure 13. The overall size of the sensor and the three versions of the sensor.

The overall combined design is shown in Figure 14.

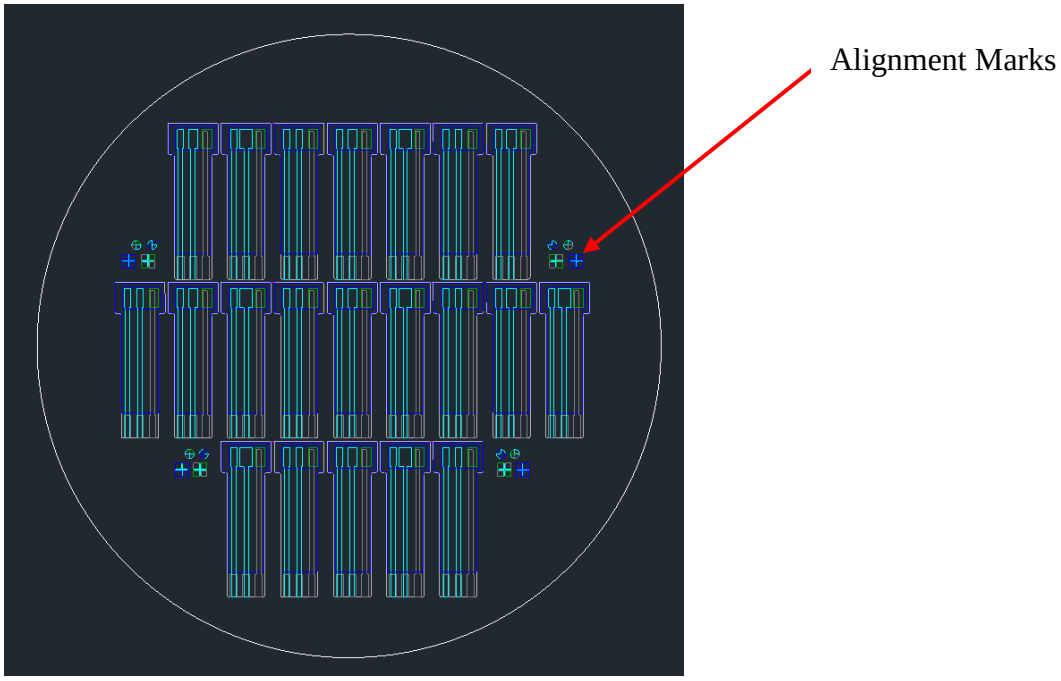

Figure 14. Overview of Entire Substrate – 0.2 mm thick Ultra High Molecular Weight Polyethylene Substrate Material.

4.6 Fabrication of the formaldehyde gas sensor using thin film technology

Based on the design described above, the formaldehyde gas sensor was fabricated using thin film technology. The reference electrode was produced using thick film printing technique.

The processing steps undertaken in this fabrication process:

Step 1 – *Laser Cut PET Substrate* – Ultra High Molecular Weight Polyethylene 0.2 mm thick – laser cut a 10.16 cm (4-inch) diameter circle of from a 300 x 300 mm sheet of 0.2 mm thick U.H.M.W polyethylene film (Goodfellow ET301200, order code 806-710-80). The substrate was cut into a round shape to facilitate the spinning of photoresist onto it during the photolithography patterning steps.

Step 2 – *Tack Down One Substrate to Rigid Base Substrate* - Adhere one of the laser cut substrates to a 0.5 mm thick alumina substrate. The 0.2 mm PET substrate was not rigid and photoresist may not spin evenly on the surface. It was decided to bond it to a rigid 0.5 mm thick alumina substrate to determine if it would produce a sharper image during photolithography. The laser cut PET substrate was bonded to the alumina substrate using a Wafer – Mount 562 pre-form (SPI Supplies, West Chester, PA 19380).

Step 3 – *Spin Coat Photoresist* - Spin coated photoresist S1818 (MicroChem Corp., Westborough MA 01581) onto the PET substrate mounted onto alumina and the unmounted PET substrate. The photoresist was cured on a hotplate at 115 °C for 75 seconds.

Step 4 – *Expose Photoresist* - Using an ABM mask aligner and the darkfield photomask with the pattern for the palladium electrodes the photoresist layer was patterned for lift-off (see Figures 15a and 15b). The exposure time was 6.5 seconds.

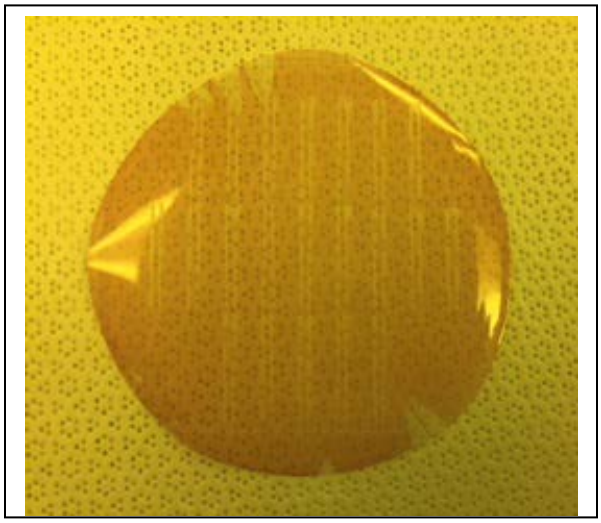

Figure 15. (a) Unmounted PET Substrate coated in photoresist, exposed with palladium electrode photomask and developed.

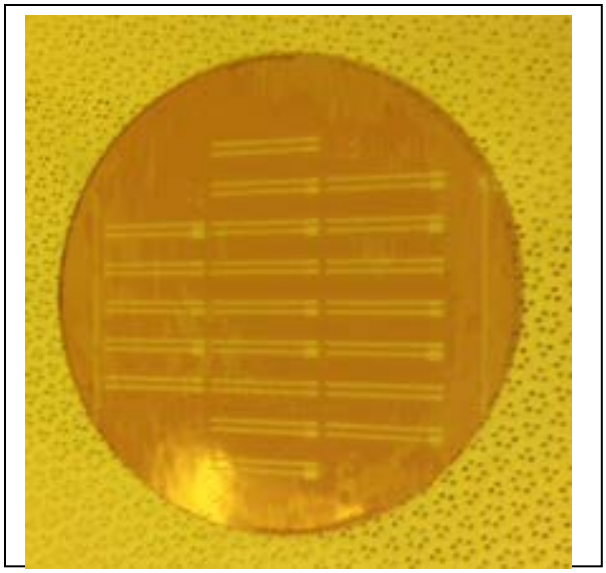

Figure 15. (b) PET Substrate mounted to alumina substrate coated in photoresist, exposed with palladium.

Step 5 – *Develop Photoresist* - Microposit 351 Developer ((MicroChem Corp., Westborough MA 01581) was used to develop the palladium electrode pattern on the PET substrates. The substrate was rinsed thoroughly in deionized water and blew dry with ultrahigh purity nitrogen. Microscope was employed to inspect pattern ensuring that pattern produced correctly in photoresist at selected exposure time. The substrate was then placed in an oven at 115 °C removing residual deionized water from photoresist for 30 minutes.

Step 6 – *Tape Down Unsupported PET Substrate* – In order to have an even layer of metal be sputtered onto the unsupported substrate needed to lay flat. The PET substrate was

mounted onto a 6” diameter silicon substrate that was covered in aluminum foil using Kapton tape

Figure 16. Unmounted PET substrate held down flat using Kapton tape prior to being introduced into sputtering machine.

Step 7 – *Sputter Titanium/Palladium on Unsupported PET Substrate* –Unsupported, photoresist patterned PET substrate was loaded into Discovery 18 DC magnetron sputtering machine (Denton Vacuum, Moorestown, NJ 08057). The sputtering machine was pumped down until a high vacuum, 2.5 x 10^{-6} torr was reached. In order to increase adhesion of metal layer to plastic substrate, a 60 second RF plasma pre-clean step was first performed. 100 Å of titanium was first sputtered as an adhesion layer. Then 1000 Å palladium was sputtered onto PET substrate (see Figure 17).

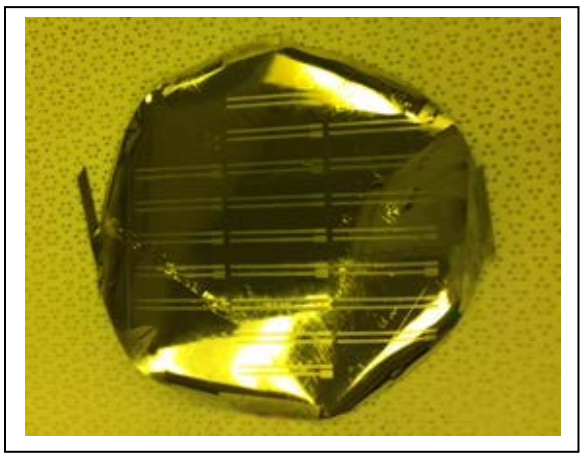

Figure 17. Patterned PET Substrate coated in titanium and palladium.

Step 8 – *Complete Lift-Off Process to Form Electrodes* – Metal coated PET substrate was submerged in a container filled with acetone removing photoresist. The container was placed in an ultrasonic bath. This bath step used approximately five minutes. The working and the counter electrodes were the palladium thin film. The substrate was

then rinsed thoroughly in deionized water and blew dry with ultrahigh purity nitrogen. Put substrates in oven at 115 °C to dry for 10 minutes (see Figure 18).

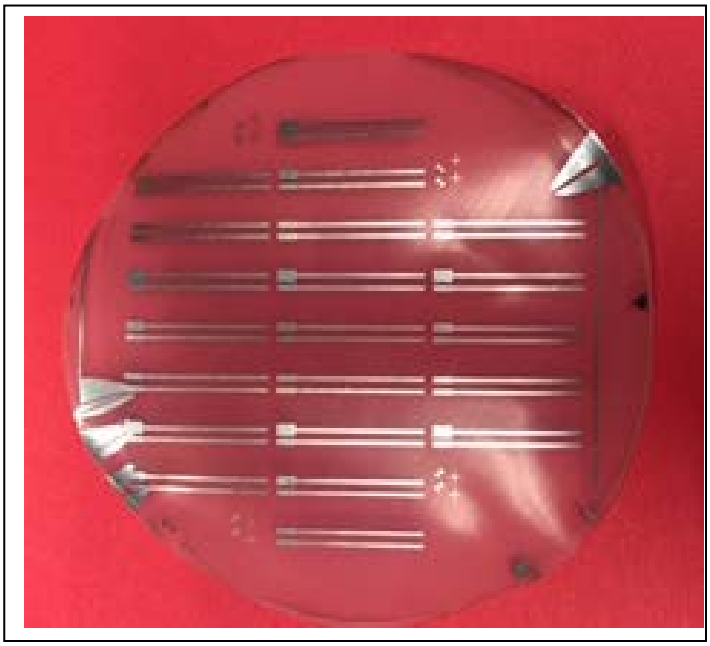

Figure 18. PET Substrate with palladium working and counter electrodes.

Step 9 – *Quality Control* – Test was taken ensuring that the metal layers do not delaminate from PET substrate by putting a piece of Scotch tape on top metal layer and pulling. Metal layers do not pull off demonstrating that RF pre-cleaning step and titanium thickness are adequate to insure palladium adherence to PET. Inspection of the pattern showed good pattern transfer. There was unwanted metal near the edges of the PET substrate where the photoresist did not spin coat well. This was due to the unmounted substrate not being very rigid.

4.7 Thick film printing of Ag/AgCl reference electrode

The Ag/AgCl reference electrode of this formaldehyde gas sensor was fabricated by thick-film technique. The PET substrate with thin film deposited palladium working and counter electrodes (Figure 11) was then processed in the following steps:

1) The PET substrate that was adhered to an alumina base will have titanium/palladium sputtered onto it and then lift-off completed.
2) The PET substrates then went through thick film printing process. The layers for thick film printing were:
    a. Bonding Pad Reinforcement - 126-33 – Extremely Conductive Ink -Silver Ink (Creative Materials, Ayer, MA 01432)
    b. Reference Electrode - 113-09(S) - Chemically Resistant Electrically Conductive Medical Electrode Ink – Silver/Silver Chloride Ink (Creative Materials, Ayer, MA 01432)
    c. Insulation Layer - 126-44 - Dielectric Ink – Insulation Ink (Creative Materials, Ayer, MA 01432)
3) Individual electrodes will be cut from the thick film printed PET substrates.

In summary, we have completed our assigned research under this sub-contract. We have successfully developed the sensor prototypes for acrolein and formaldehyde gas detection. We also have performed testing on the acrolein sensor prototype using differential pulse voltammetry (DPV) transduction technique. The complete formaldehyde gas sensor prototypes have been sent to our collaborator in NASA and Makel Engineering Inc. for evaluation. The electronic inter-phase for these acrolein and formaldehyde gas sensors was considered more difficult for our developed sensor prototypes, and the researchers decided to use the MASA's SiC based sensor prototypes for the overall sensor system. Our research was considered a technical success and completion under this subcontract.

5. SIC BASED SCHOTTKY DIODE GAS SENSORS FOR DETECTION OF METHANE, FORMALDEHYDE AND ACROLEIN

5.1 Sensor Fabrication

NASA Glenn Research Center has previously demonstrated prolonged stable operation of gas sensing SiC-based Schottky diodes at elevated temperatures. These Schottky diodes use palladium oxide (PdO_x) as a barrier layer between a catalytic sensing metal, such as palladium (Pd), platinum (Pt), or an alloy, and the silica carbide (SiC) substrate. The PdO_x barrier layer is intended to prevent silicide-forming reactions between the precious metal and the SiC [Hunter et al., 2008a, 2008b; Xu et al., 2012]. The basic design of the Catalytic metal/PdO_x/SiC Schottky diode sensing element is illustrated in Figure 19 [Hunter et al., 2008b]. The sensor is fabricated using an n-type SiC wafer, with an n-type epilayer. The wafer is first prepared by cleaning, followed by sputter depositing titanium and nickel to form the backside contact. The front side of the wafer is patterned with a photoresist/mask pattern for liftoff deposition of PdO_x and catalytic metal. Reactive sputter deposition of approximately 50 Å of Pd in oxygen/argon gas leads to the PdO_x barrier layer. Sputter deposition of the catalytic sensing layer (~450 Å) is on top of this barrier layer. A forward or reverse bias may be applied to the diode through the catalytic metal layer causing forward or reverse current to flow. The PdO_x barrier layer is thin enough such that tunneling can occur through this layer forming the Schottky diode structure.

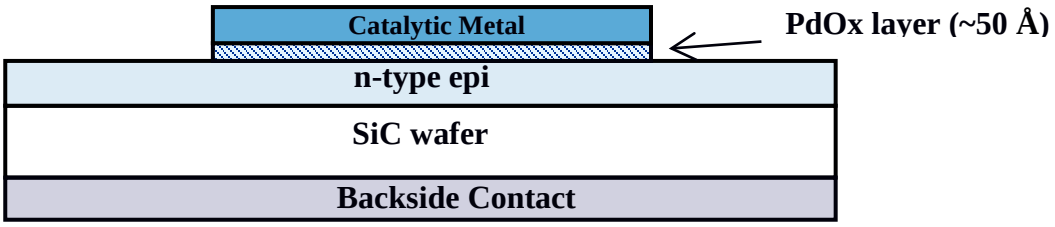

Figure 19. Illustration of the Pd/PdO_x/SiC Schottky diode gas sensor. A catalyst is located above barrier layer (PdOx) on the SiC substrate. The backside contact and gate form the two electrodes of the diode [Hunter et al., 2008b].

Figure 20a shows a picture of a single PdO_x/SiC based diode fabricated using sputtering techniques. The center circle is a Pt/PdO_x/SiC diode, which can have a radius 250-500 µm, while the surrounding area is SiC semiconductor. The size of the sensors structure is shown in comparison to a dime in Figure 20b. Testing of this diode before packaging is accomplished by mounting the backside metalized (Ti/Ni) diode on a gold foil and making contact to both the front and back sides of the diode on a probe station.

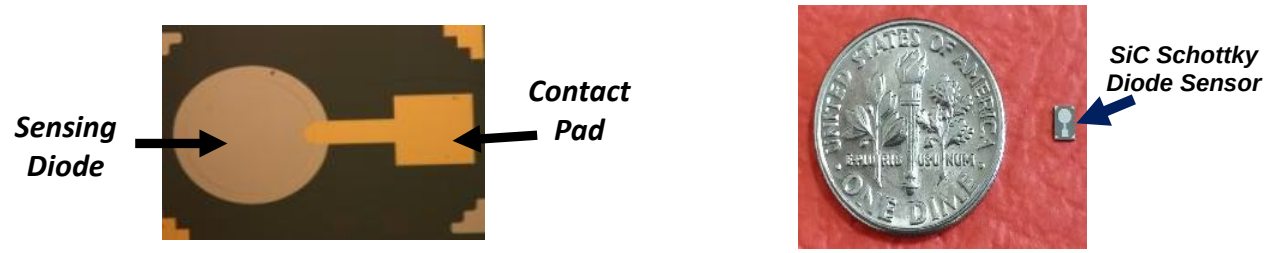

Figure 20. (a) A microscope image of a single PdO_x/SiC based diode with both a contact pad (where electrical connections are made) and a sensing diode. The sensor pad as fabricated has as a 230-500 microns radius. (b) Comparison of Schottky diode sensor to a dime.

The implementation of the sensor into a system includes integration of a temperature detection and heater. Figure 21 shows the mounting of a Schottky diode sensor onto a heater substrate for temperature control, and Figure 21b shows mounting of the packaged sensor onto a probe head for measurement of emissions from aeronautic engines [Xu et al., 2012].

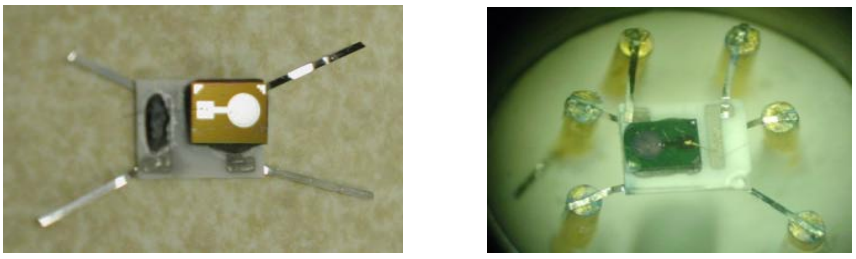

Figure 21. (a) Mounting of a sensor element onto a heater substrate. (b) Sensor and heater substrate mounted onto a probe head for use in emission monitoring [Xu et al., 2012].

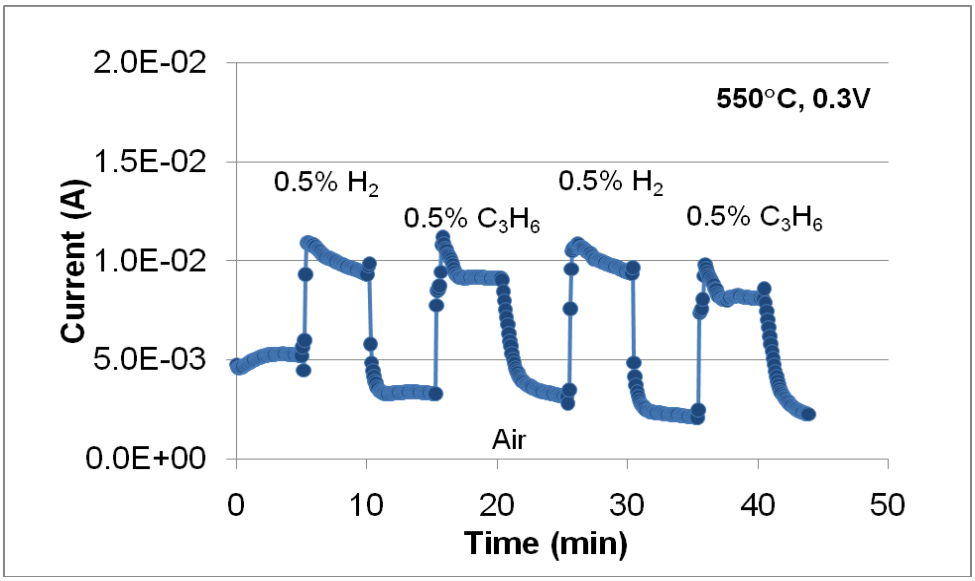

Figure 22. A Pt-PdOx-SiC sensor operated at 550°C, 0.3 V for 0.5% H_2 and 0.5% C_3H_6 detection. Air is used for the baseline [Xu et al., 2012].

This core configuration is adaptable and able to detect a range of species through adjusting both temperature and the catalytic sensing metal. Testing has shown a $Pd/PdO_x/SiC$ structure provides stable sensing of hydrogen (H_2) and hydrocarbons (C_xH_y) at high temperatures, while also being operational over a wide temperature range. For example, such a sensor was tested at 450°C for nearly 1500 hrs, and detection of hydrogen from room temperature to 500°C was also achieved [Hunter et al., 2008b]. The sensor to measure hydrogen down to the level of 250 ppb in air was also achieved [Hunter et al., 2008b]. In particular, at high temperatures the sensors can respond a broad range of hydrocarbons. Figure 22 shows the sensor response of Pt/PdOx/SiC diode in air, 0.5% hydrogen (H_2) and 0.5% propylene (C_3H_6) [**Error! Bookmark not defined.**]. Since the temperature is high enough such that both hydrogen and propylene can dissociate on the catalytic metal for detection, both species can be detected and with nearly the same response. As the temperatures is lowered, more stable species, such as methane, are not detected while species such as hydrogen can still be measured. This capability of the sensor is core to the approach used to selectively detect methane, acrolein, and formaldehyde for this application.

One of the major steps in developing an approach to selectively measure methane, acrolein, and formaldehyde in a mixed atmosphere was the investigation of ruthenium palladium (RuPd) as a sensing alloy. The catalytic sensing layer on the PdOx/SiC diode structure was formed by sputtering from a Ru92Pd7 target. It was founded 75°C the sensor detected acrolein but did not contact formaldehyde or methane (see Section 5.3 below). In conjunction, the Pt/PdOx/SiC diode sensor structure was found to detect both formaldehyde and acrolein, but not methane at 75°C, while this is the structure type in all three species that near 500°. These results are summarized in Table 2. Thus, if a sensor array a Pt/PdOx/SiC diode sensor at 500°C, a second Pt/PdOx/SiC diode sensor at 75°C, and a RuPd/PdOx/SiC sensor at 75°C, the combination of these three sensor responses can be used to determine methane/hydrocarbons, formaldehyde, and acrolein concentrations independently.

Table 2. Catalytic sensing metal and operating temperature approach to determine methane, formaldehyde and acrolein using a PdOx/SiC structure.

Target Gases	Catalytic Sensing Metal	Operating Temperature
Methane and other hydrocarbons detection including Formaldehyde and Acrolein,	Pt	~500°C
Formaldehyde and Acrolein, but Not Methane Detection	Pt	75°C
Acrolein Only Detection	RuPd	75°C

5.2 Testing System

The array of gas sensors were tested on an MMR Technologies probe station. Three sharpened probe tips were available with manual x, y and z translation to make contact with the electrodes. Good contact was attained by placing the probe tip onto the electrode material and tightening it so that the probe visibly, but minimally, flexed. Backside electrodes were connected to by laying the sensor onto a piece of gold foil and making contact to the foil. The sample and backside electrode were supported on a hand-made heater with a ceramic top to avoid grounding or interference through the heating elements. An IR remote temperature measurement gun was

used to measure the temperature at a sensor element surface at various voltage inputs to the heater stage with the observation window removed. As an example, 20 volts run to the heater provided a sensor surface temperature of 75ºC. The power supply voltage was then used to achieve the surface temperature setting when the observation window was needed in place to maintain gas concentration.

Gas was introduced into the test cell through the gas port seen in Figure 23 to the left of the observation port. The ball valve could be closed to close off the gas supply and allow the sensor to dwell in a quiescent environment. MKS mass flow controllers were used to provide flow control and purging of the cell. Gas cylinders of 2 and 10 ppm acrolein and 5 pm formaldehyde were used. All 3 cylinders came with a calibrated measured concentration. Cylinders of air and nitrogen were used for purging and background measurements.

Measurements were made with a CH Instruments 660C electrochemical analyzer. The analyzer was electrically attached to the probe tips through electrical feedthroughs on each probe. The CH Instruments software interface was used to run cyclic voltammetry, differential pulsed voltammetry and I-t curves to test the activity of the sensor elements during exposure to test gases.

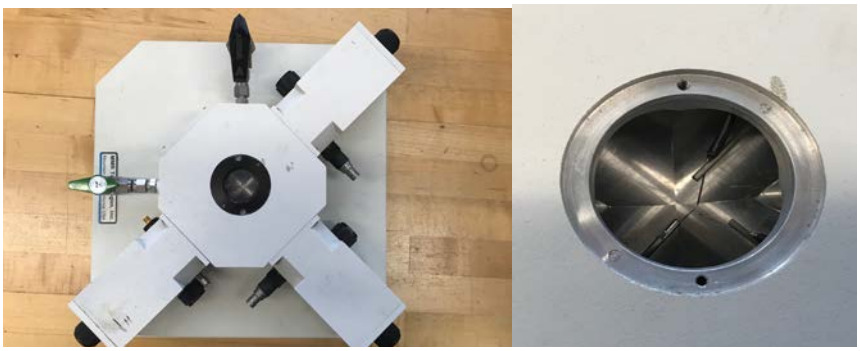

Figure 23. The probe station. The heating stage is inserted from the top left corner of the main body (not shown). In the close up of the observation port, the probes can be seen.

5.3 Test Results

As noted above, a Pt/PdOx/SiC Schottky diode operated at 500°C. can detect a broad range of hydrocarbons including methane, formaldehyde, and acrolein. Separate tests have shown consistently that at lower temperatures (e.g., below 200°C) the Pt/PdOx/SiC Schottky diode sensor does not detect methane. However, core to the viability this approach is the capability to also differentiate between formaldehyde and acrolein. A number of experiments were run at different temperatures to determine the combination of temperatures and sensing alloys to allow this differentiation. A summary of the results of this work is shown in Figures 24-25, which shows the current-voltage response of Pt/PdOx/SiC Schottky and Ru7Pd93/PdOx/SiC diode sensors in a nitrogen (N_2) background.

In particular, Figure 5 shows the ability of the Pt/PdOx/SiC Schottky diode to detect formaldehyde and acrolein at 75° C. Thus, Figure 24 shows the Pt/PdOx/SiC Schottky diode capability to measure both formaldehyde and acrolein. In general, such a response is expected for sensors of this type in which more volatile hydrocarbon species are disassociated at lower temperatures, while both volatile and more stable species are disassociated at higher temperatures.

Figure 25 shows the response of a Ru7Pd93/PdOx/SiC Schottky diode to formaldehyde and acrolein. The change in sensing alloy from Pt to RuPd has a notable effect on the sensing response and selectivity to acrolein. In particular, at these temperatures, the RuPd alloy does not respond to formaldehyde but does respond to acrolein.

Thus, this data supports the approach suggested in Table 1 that the combination of Pt/PdOx/SiC Schottky diodes at two different temperatures combined with Ru7Pd93/PdOx/SiC Schottky diode at a lower temperature provides the capability to differentiate between these three stations. These sensors were then fabricated as needed and supplied to Makel Engineering, Inc. Implementation and calibration of these sensors into an overall test system templates took place as an activity in that part of the project.

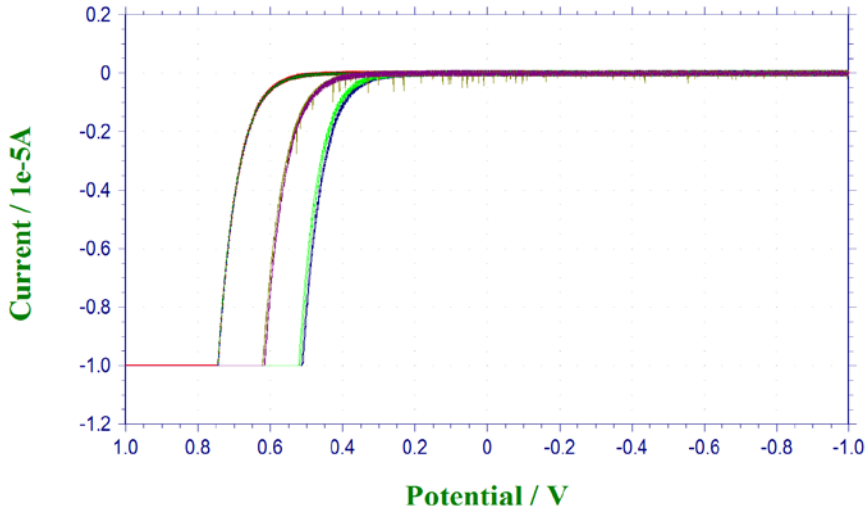

Figure 24. Pt/PdOx/SiC Schottky diode at 75°C responding to 5 ppm formaldehyde (blue), N2 (red), and 2 ppm acrolein (green). The background gas is nitrogen.

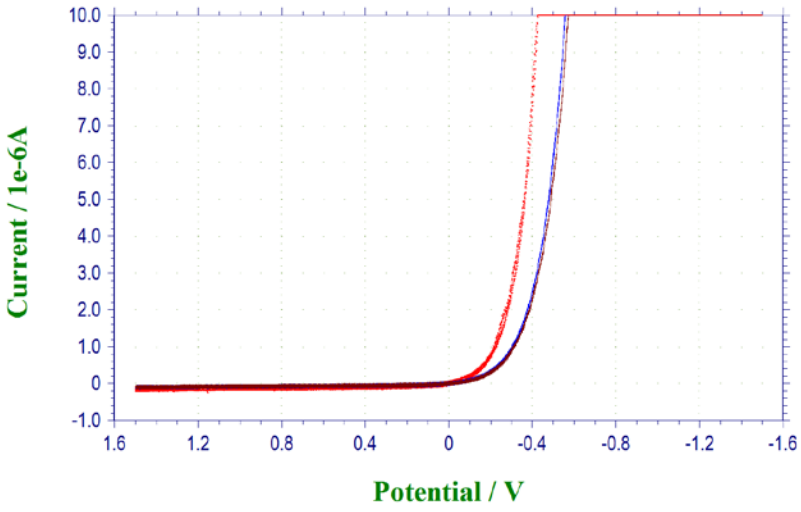

Figure 25. Ru7Pd93/PdOx/SiC Schottky diode at 75°C responding to 2 ppm acrolein (red). The formaldehyde and N2 signals overlap (blue and brown) suggesting that the Ru7Pd93/PdOx/SiC does not respond to formaldehyde at these temperatures. The background gas is nitrogen.

6. SYSTEM INTEGRATION

6.1 Introduction

Prototypes combining particulate and chemical sensors have been developed, based on two prototype designs: Prototype I and Prototype II. Prototype I units were built with particulate, CO, O_2 and hydrocarbon sensors. Prototype II units were built with additional acrolein and formaldehyde sensors.

Both prototypes versions are handheld, include data logging, and user alarms to measurements are outside of safe ranges. The CO and O_2 sensors are provided by MEI. The hydrocarbon acrolein and formaldehyde sensors will be provided by NASA and packaged by MEI. The particulate sensors are provided by NASA and integrated into the prototype by MEI with the housing provided by CWRU.

This report focuses on MEI's activities.

6.2 Prototype I

This section describes the Prototype I units. Table 3 lists the key prototype specifications. Figure 26 shows the prototype, illustrating the key components.

Table 3: Prototype I Specs

Spec	Description
Species	O_2, HC, CO, and particulate
Size/ Weight	Handheld <1 lb (without battery)
Battery Powered	11.25V Rechargeable Li-Ion 2.95Ah
Datalogging	Continuous for all sensors $\geq$ 1 recording per minute
Touch Display Screen	3.2" LCD Backlit Resistive Touch Display
Alarms	Screen Indications, red LED
Intake	Blower for particulate, diffusion for chemical sensors
Operating Temp	-20 to 50°C
Humidity	0 to 5% relative humidity, non-condensing
Communication	USB, Data Download

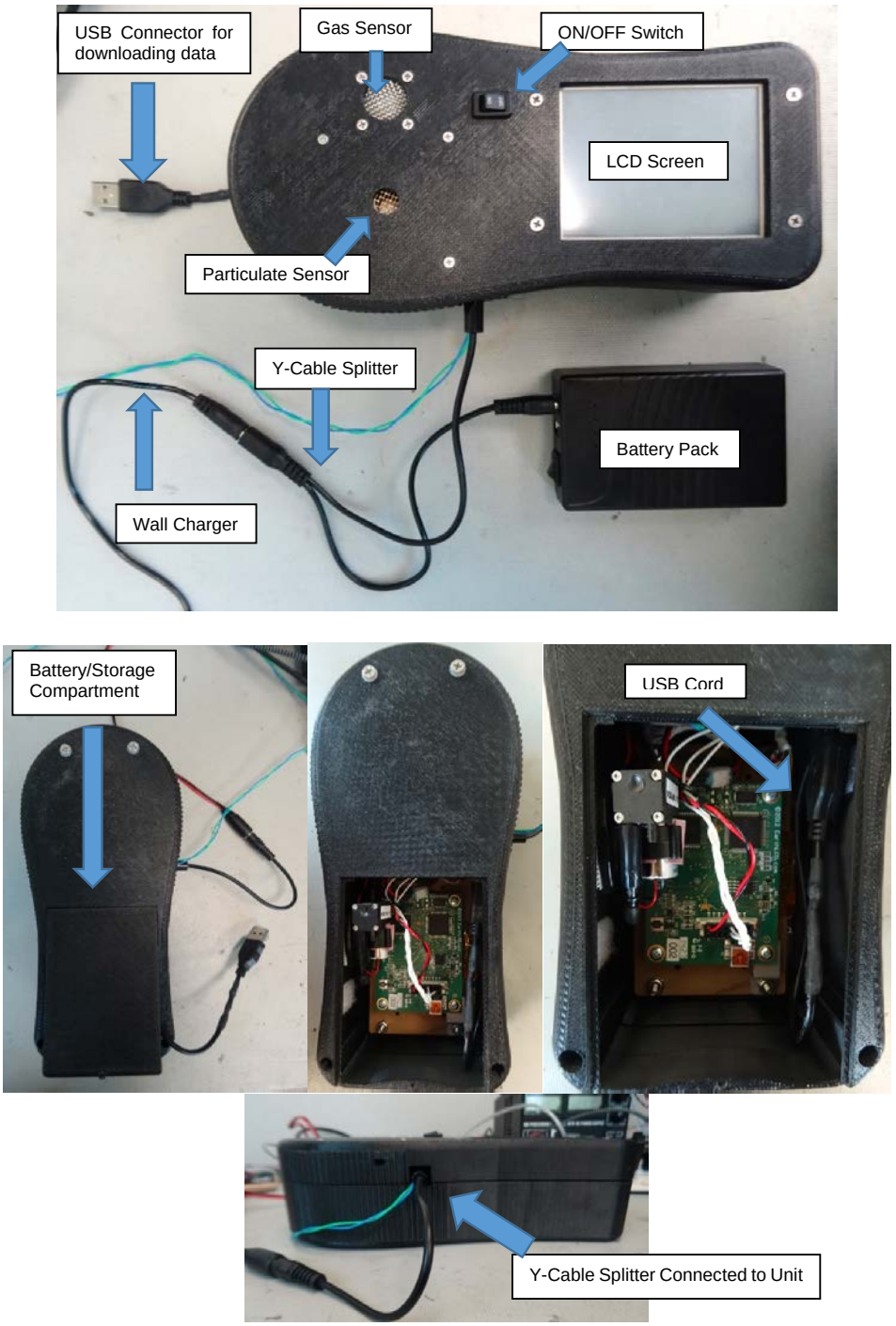

Figure 26. Prototype 1 component overview.

Prototype I - LCD Screens and Transitions

MEI has developed the framwork for the LCD screen states for the system. The diagram in Figure 27 illustrates the various screens within the LCD user interface and how the system

transisitons to different screens and states. Each screen and the transition triggers are described in more detail below. In order to facilitate rapid prototyping of the hardware for this prototype design, the physical warning LEDs and buttons are emulated as annunciators and onscreen buttons on the LCD touch-screen. Words enclosed between "< >" symbols indicate an onscreen button. Words in Italics indicate a selection or editable fields

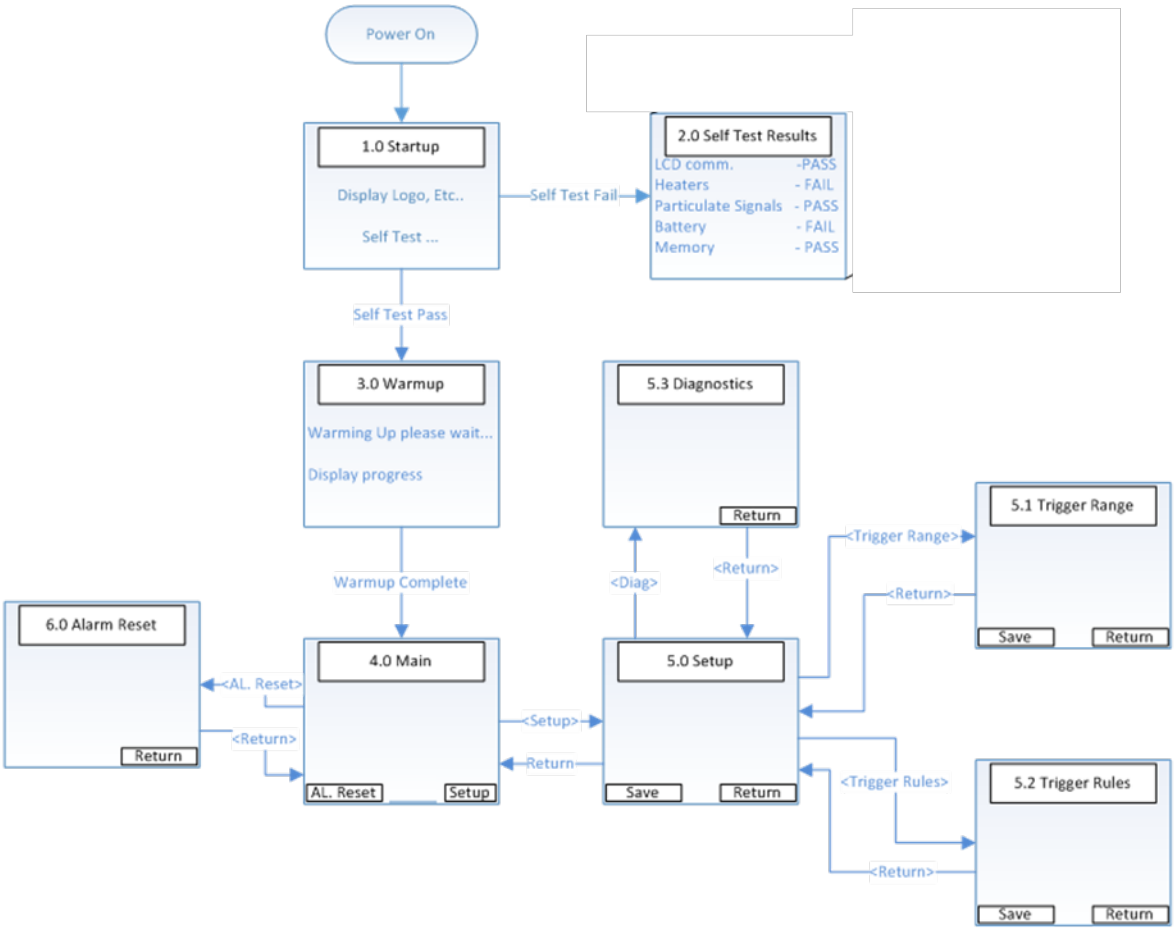

Figure 27. LCD screen and state transition diagram.

Screen 1.0 Startup

This screen (Figure 28a) appears on power up, displaying the system name, logo and version. The display transitions to Screen 2.0 *Self Test Results*.

Screen 2.0 Self-Test Results

The Self-Test Screen (Figure 28b) checks the battery life and that the LCD is communicating with the system. If no fault is detected the display transitions to screen 3.0 *Warmup*.

Screen 3.0 Warmup

If the system passes the self-tests, it transitions to the Warmup Screen (Figure 3c). The LCD issues the commands to power up the sensors and begin warming up and stabilizing the sensors. The percentage of progress is indicated. When the warmup and initialization is complete the system transitions to Screen 4.0 Main.

(a) (b) (c)

Figure 28. LCD screens: a) Start Up, b) Self-Test, c) Warm Up.

Screen 4.0 Main Menu

This the main operation screen during normal operation. This screen (Figure 29) displays the measurements from the chemical and particulate sensors. There are 3 onscreen buttons. If one or more measurements triggers an alarm, a global annunciator virtual LED appears and the color of the background for the sensor measurements is changed according to the criteria set from the Setup Screen (see next). The onscreen buttons are <Alarm_Reset>, and <Setup>. Once triggered, the alarm annunciators will remain active until they are reset by pressing <Reset Alarm> and making the desired selections from the alarm reset screen. Pressing <Setup> brings up the Setup Parent Screen.

Figure 29. LCD screen – Main Menu.

Screen 5.0 Setup Parent

This screen is entered from the <Setup> button from the Main Screen to allow the user to configure the system alarm trigger range and rules, as well as other operating parameters. This screen is the parent of three child screens to allow detailed configuration and diagnostics. The options on this screen are: *Trigger Range*, *Trigger Rules*, *Sleep Time*, *Operating Mode*, Diagnostics, and *Return*. <Trigger Range> opens Screen 5.1 described below. <Trigger Rules> opens Screen 5.2 described below. Pressing <Diagnostics> displays screen 5.3 described below. *Sleep Time* allows the user to enter a time out period before the LCD goes into low power mode and turns off the backlight. The *Operating Mode* field selects between normal and low power operation profiles. Changes made to this screen are kept by pressing <Save>. Pressing <Return> takes the user back to Screen 4.0

Screen 5.1 Setup Alarm Trigger Range

This screen (Figure 30b) is displayed when <Trigger Range> is pressed on Screen 5.0 (Figure 5a). It allows the user to enter the range of measurement of each sensor that triggers an alarm condition for each sensor. Enter any changes and press <Return> button to save any changes and return to the Setup Parent Screen (Figure 5a).

Screen 5.2 Setup Alarm Trigger Rules

This screen (Figure 30c) is displayed when <Trigger Rules> is pressed on Screen 5.0. It has selections for setting trigger actions for the buzzer and on screen annunciators. The <Return> button saves any changes and returns to the setup screen (Figure 30a).

(a) (b) (c)

Figure 30. LCD screens: a) Setup, b) Trigger Range, c) Trigger Rules.

Screen 6.0 Alarm Reset

This screen (Figure 31) is entered when <Reset Alarm> is selected from Screens 4.0. This screen allows clearing alarm audio and visual annunciators. The user can select one or more sensor alarms to reset. <Return> takes the user back to Screen 4.0.

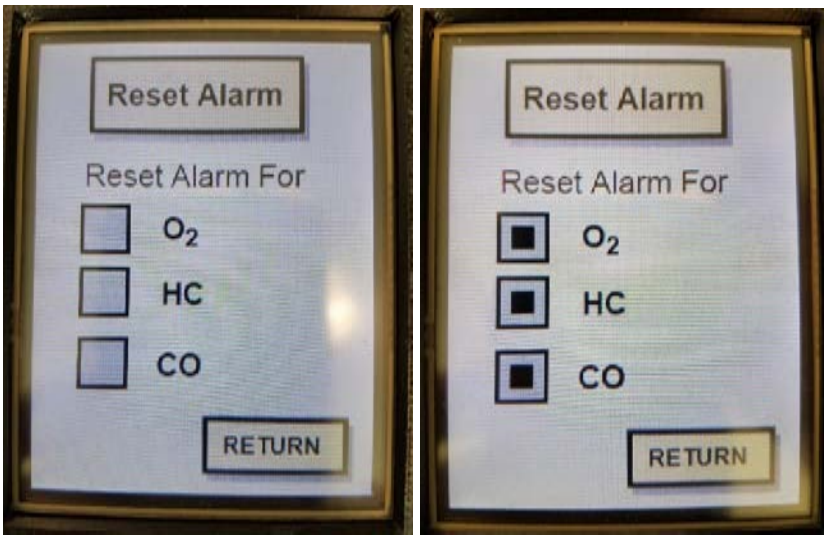

(a) (b)

Figure 31. Reset alarm screens: a) no sensors selected to reset, b) all sensors selected to reset.

Windows Based Graphical User Interface (GUI)

In addition to the LCD GUI for real time data display, a Windows based GUI has been developed. The key functionalities of the GUI include:

1. Validate communication between the various components of the entire system.
2. Manipulate the data logging functionality (Enabling/Disabling).
3. Change the parameters for the particulate sensor equation during run-time.
4. Allow the user to retrieve and download logged data from the ARM microcontroller.

Figure 32 shows the layout of the GUI that enables the user to interact with the prototype electronics and the built-in data logging functionality. Each section of the GUI (Figure 8-Figure 11) is explained in further detail). The section shown in Figure 33 illustrated where the data sent and received from the unit is displayed. This section has the following fields:

1. **Received Area:** Will display all incoming data (responses) from the prototype.
2. **Sent Area:** Will display the data that is sent to the prototype to invoke a response from it.
3. **Clear Button:** Will clear the Received box from all data.

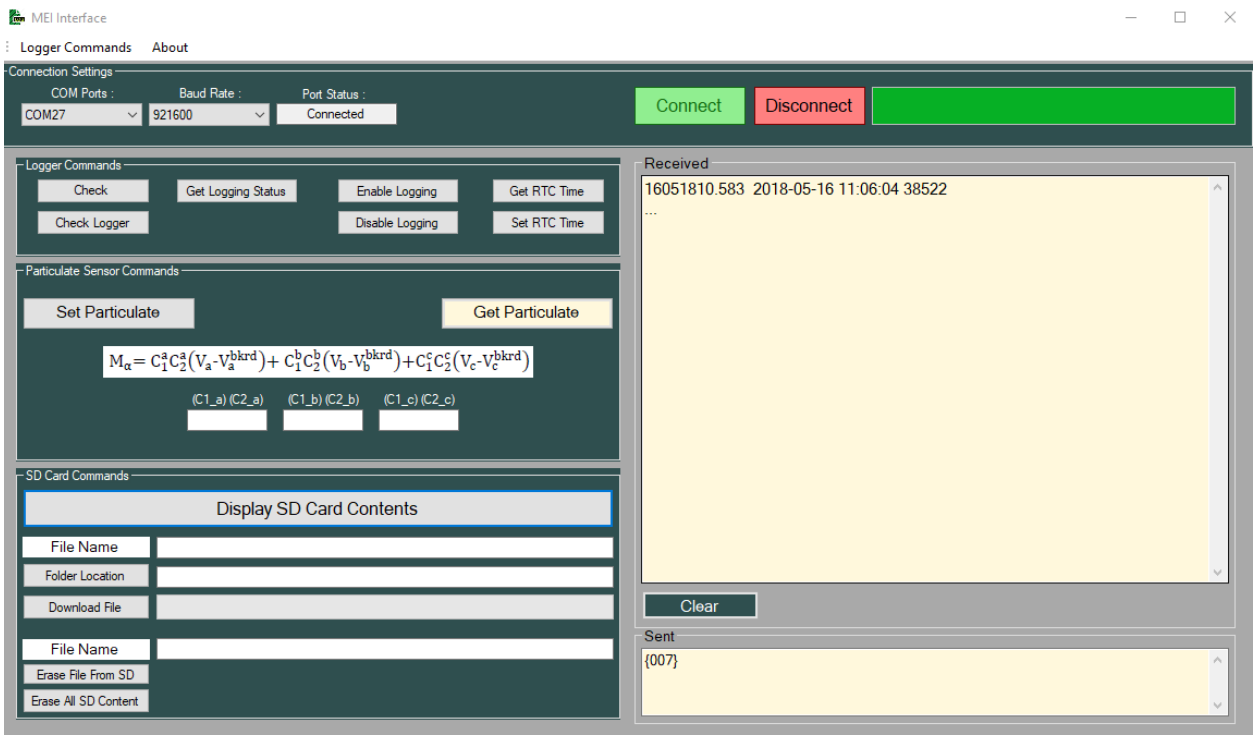

Figure 32. Layout of the windows interface.

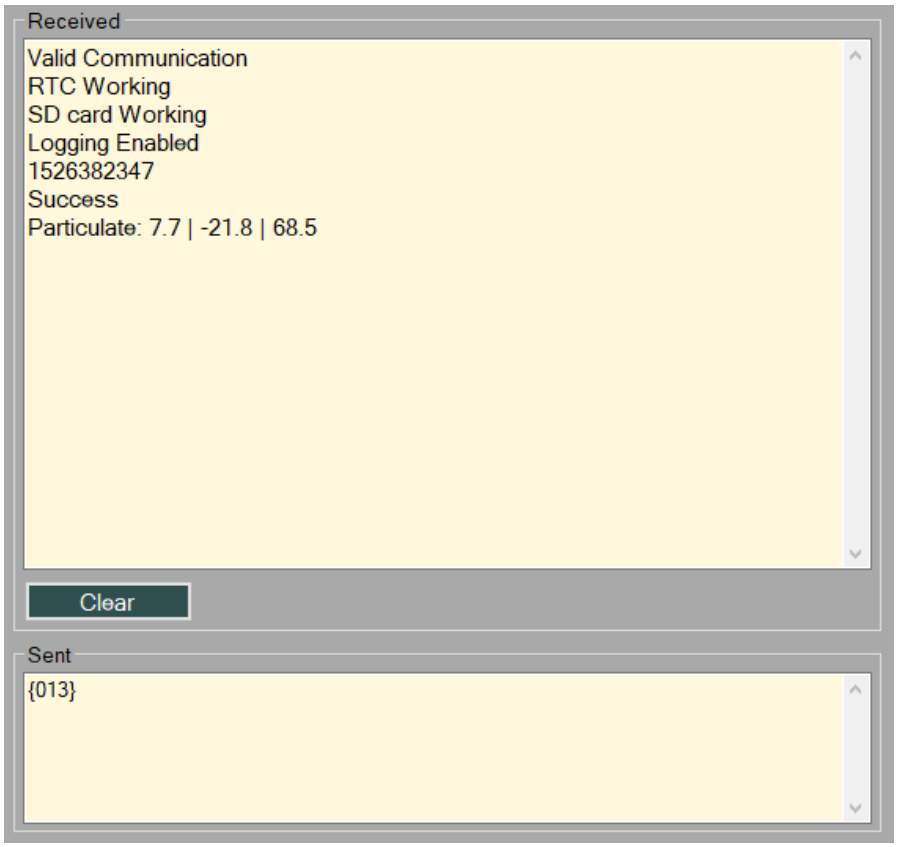

Figure 33. Data display fields.

Figure 34 shows the section focused on logger commands. The functionality of each button is described below.

1. **Check:** Validates Communication between the PC interface and the ARM microcontroller.
2. **Check Logger:** Confirms that the SD card is attached to the Logger and that the RTC (real time clock) is functioning correctly.
3. **Get Logging Status:** Indicates if the logger is currently logging data.
4. **Enable Logging:** Enables logging so that data can be recorded on the SD card.
5. **Disable Logging:** Disables logging so that data will not be recorded on the SD card.
6. **Get RTC Time:** Returns the current Real Time Clock Time from the logger board.
7. **Set RTC Time:** Retrieves the current time from the host machine (computer) and sends the time to the logger board. The logger board will update its RTC internally.

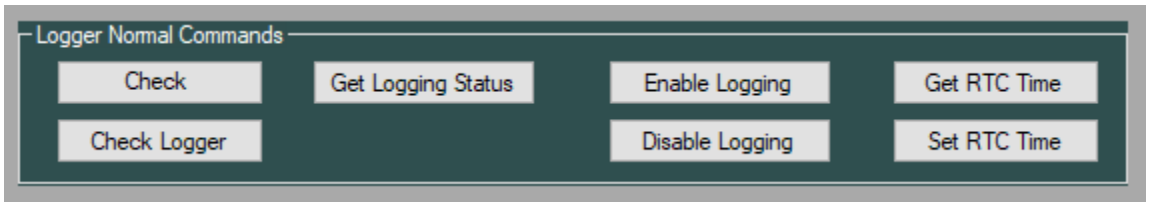

Figure 34. Logger normal commands.

Figure 35 shows the Particulate Commands section. The focus of this section is to set the coefficients for the particulate sensor.

1. **Get Particulate:** Retrieves the current particulate coefficients stored in the prototype non-volatile memory. The default at power up and device reset is: **7.7 | -21.8 | 68.5,** those values correspond to these components in the equation: $C_{1a}C_{2a}$, $C_{1b}C_{2b}$, $C_{1c}C_{2c}$.
2. **Set Particulate:** Sets the $C_{1a}C_{2a}$, $C_{1b}C_{2b}$, $C_{1c}C_{2c}$ parameters of the particulate sensor equation, when different values, other than the default, are inserted in the boxes.

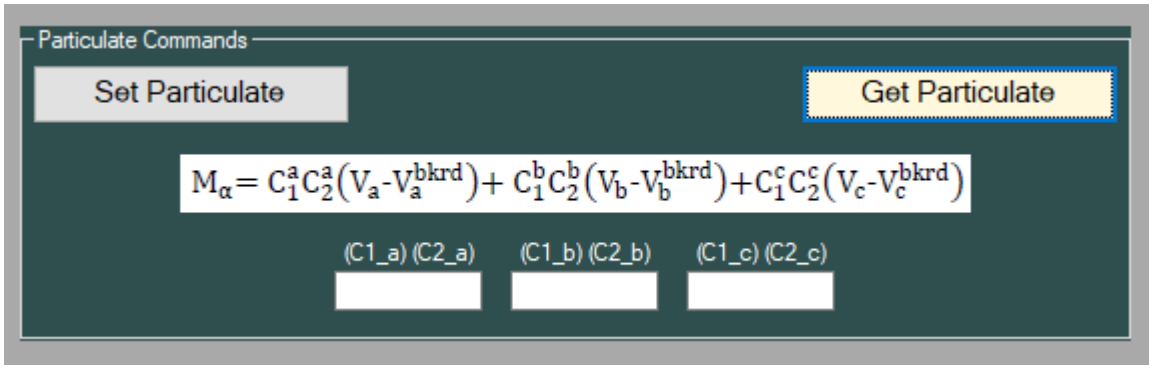

Figure 35. Particulate commands and equation.

Particulate Sensor Equation:

$$M_{\alpha} = C_{1a}\, C_{2a}\, (V_a - V_{a\_bkrd}) + C_{1b} C_{2b}\, (V_b\, V_{b\_bkrd}) + C_{1c}\, C_{2c}\, (V_c - V_{c\_bkrd})$$

Figure 36 shows the section focused on the SD card functionality. Each button and user entry field is described below:

1. **Display SD Card Contents:** Displays the files that are currently stored on the SD card with their respective date, time, and size. For example, the display shows the following:
   15101711.252 2017-10-16 12:14:16 22605
   i. 15101711.252 is the name and has the following format: ddmmyyhh.mms. (note: the 's' is the tenth place of the second value, e.g. 56 seconds is read as 5
   ii. Date and time created: 2017-10-16 12:14:16
   iii. Size: 22605 in bytes
2. **Download File:** Grabs the name of the file that is specified in the text box and downloads it to the PC machine (in this case the name of the file would be 15101711.252). Select a location for the file to download in. You must provide a location to save the file before you can download it.
3. **Folder Location:** Prompts the user to select a location to save the file to be downloaded to.
4. **Erase File From SD:** Erases the file name specified (can erase only one file at time). Erasing cannot be undone.
5. **Erase All SD Content:** Erases all the files on the SD card. Erasing cannot be undone.

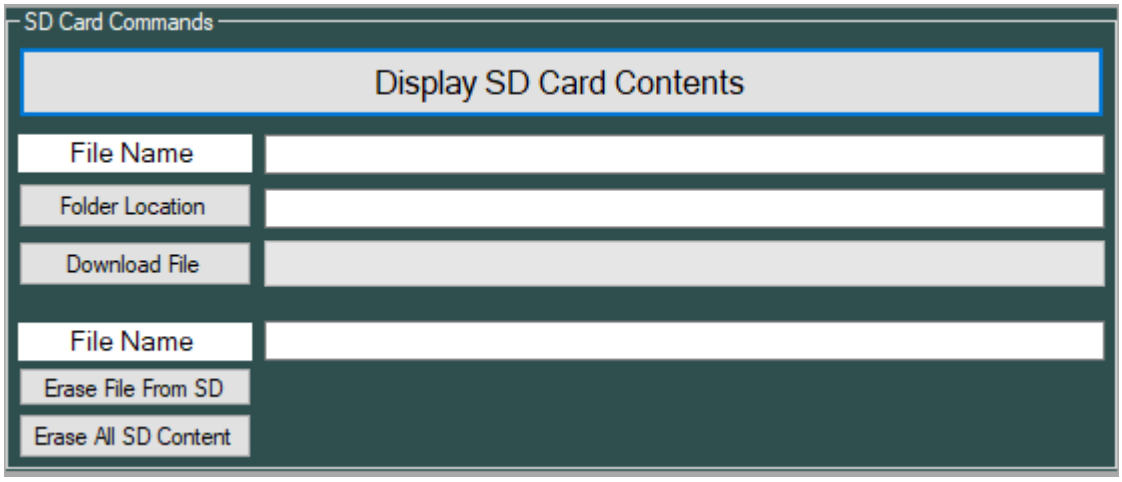

Figure 36. Logger file access commands.

6.3 Prototype II

Prototype II incorporated several improvements over the Prototype I design. In addition to the incorporation of sensors not present in Prototype I, the electronics has been updated with a higher resolution ADC. In addition, the mechanical design has been optimized to reduce the overall size. Prototype II specifications are included in Table 4.

Table 4. Prototype II Specs

Spec	Description
Species	O2, HC, CO, Acrolein, Formaldehyde, and particulate
Size/ Weight	Envelope: 8.5” x 1.8” x 4” Handheld <1 lb (without battery)
Battery Powered	11.25V Rechargeable Li-Ion 2.95Ah
Battery Life	12 Hours of Use
Datalogging	Continuous for all sensors ≥ 1 recording per minute
Touch Display Screen	3.2” LCD Backlit Resistive Touch Display
Directional Pad	Assists LCD in Navigation of LCD Menus
Alarms	Screen Indications, red LED, 95 dB buzzer
Intake Pump	3.3V Micro Diaphragm Pump up to 0.8 slpm
Operating Temp	-20 to 50°C
Humidity	0 to 5% relative humidity, non-condensing
Dust/ Water Resistance	TBD
Communication	USB, Data Download
ADC Resolution	24-bit

Overview

In Prototype II there are six different sensors that take in data. This data is then processed by an MCU and converted into engineering units such as PPM or concentration in percentage. Concurrently, these sensors have heaters built into them that are monitored to keep them at their correct respective temperatures. Once the MCU processes this data it will decide if it falls within the range set by the user. If it falls outside of this range it will signal alarms via an LED, indicators on the LCD, or a noise outputted through the buzzer. Additionally, this data will be logged internally to non-volatile memory which allows for data download via micro USB.

Prototype II has been designed to minimize overall size and improve ease of use. Having the battery plug directly into the logger board and replacing the display with a thinner alternative allows the device to be thinner than Prototype I. This design also minimizes the amount of wires needed which allows for a smaller envelope. The battery configuration also allows for easier removal and monitoring of remaining charge, as elaborated later in this document. A directional input pad has also been added to help with ease of use if the user is wearing gloves and can’t interact with the touch functionality of the display screen.

Two boards are responsible for the actions of data acquisition, processing, logging, and controlling sensor heaters. Figure 37 shows the planned system architecture, including the peripherals that each board will connect to and how they will connect to the power path.

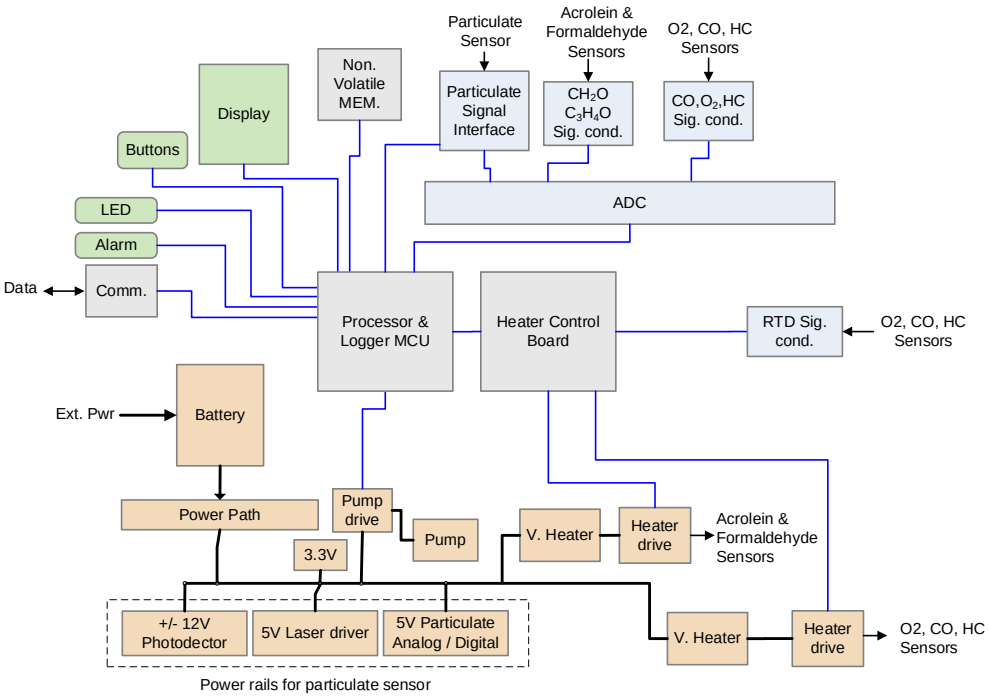

Figure 37. System architecture diagram.

The design is based around two boards connected to sensors and peripherals that are controlled and acquired by software instructions executed by the microcontrollers. There are separate signal inputs for each chemical sensor, as well as RTD inputs for the sensors that require heaters. The logger board, on the other hand, has an ADC that filters, MUXs, and amplifies signals internally. The heater control board circuitry provides software adjustable voltage for closed loop heater control using the RTD as feed-back. The heater drives are feed by the V Heater rails which are set for optimum efficiency for the chemical sensors. The pump drive circuitry connected to the logger MCU allows software control of the pump. Data is logged through the digital data bus to the non-volatile memory connected to the logger MCU. The user interacts with the device through the LCD display, buttons, LED, and alarm buzzer.

Signal Path

Figure 38 below shows an overview of the signal path between the logger and heater control boards. The signals from the chemical sensors will be connected to the logger board, while the heaters will be connected to the heater control board. The HC and CO sensors will be sharing a heater, the CH2O and Acrolein sensors will be sharing a heater, and the O2 sensor has its own heater. The logger board will communicate to the heater control board via UART1. The logger board will also be connected to the display screen via UART2.

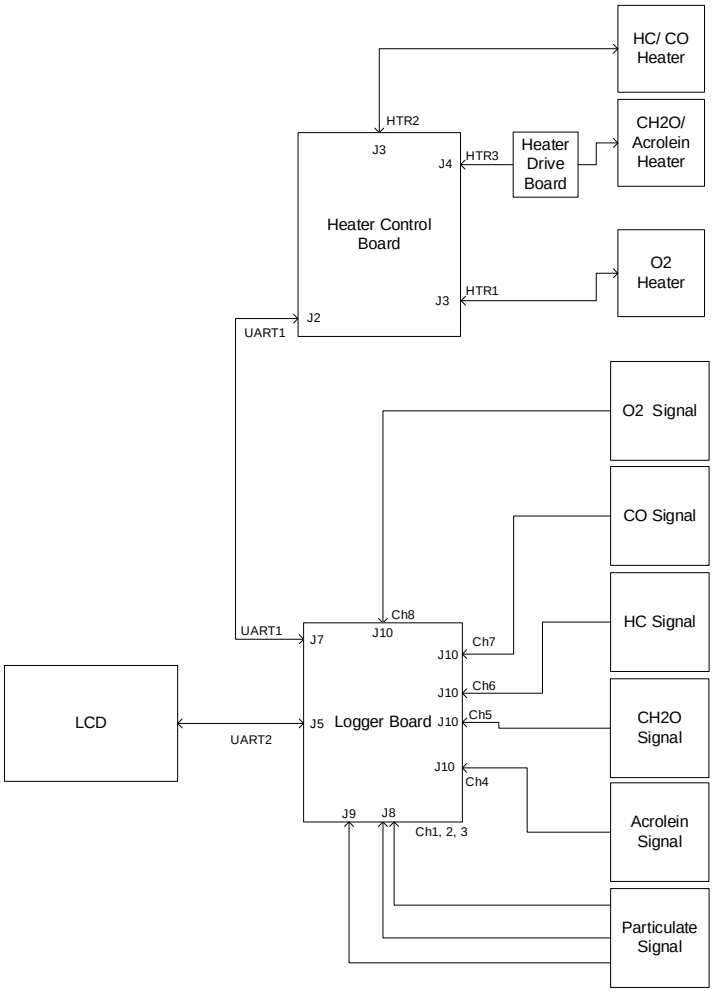

Figure 38. Signal path overview.

The signal path has been broken up into two diagrams below. Figure 39 shows how the heater control board receives RTD signals from the HC, CO, Formaldehyde, and Acrolein sensors, and the heater and current sense from the O2 sensor to find resistance. The RTD signals get filtered, sent through a mux, and then amplified. This information is then used to control the heaters and is passed along to the logger board to be stored. The logger board receives raw signal data from the six chemical sensors and converts that signal into engineering units. Figure 40 shows how the raw signals are fed through the onboard ADC. This ADC internally filters, amplifies, and picks between the different input channels. This processed data is then outputted to the MK66 MCU (not pictured) where it is further processed to find counts and concentration. This data is stored and outputted to the display screen along with the data received from the heater control board.

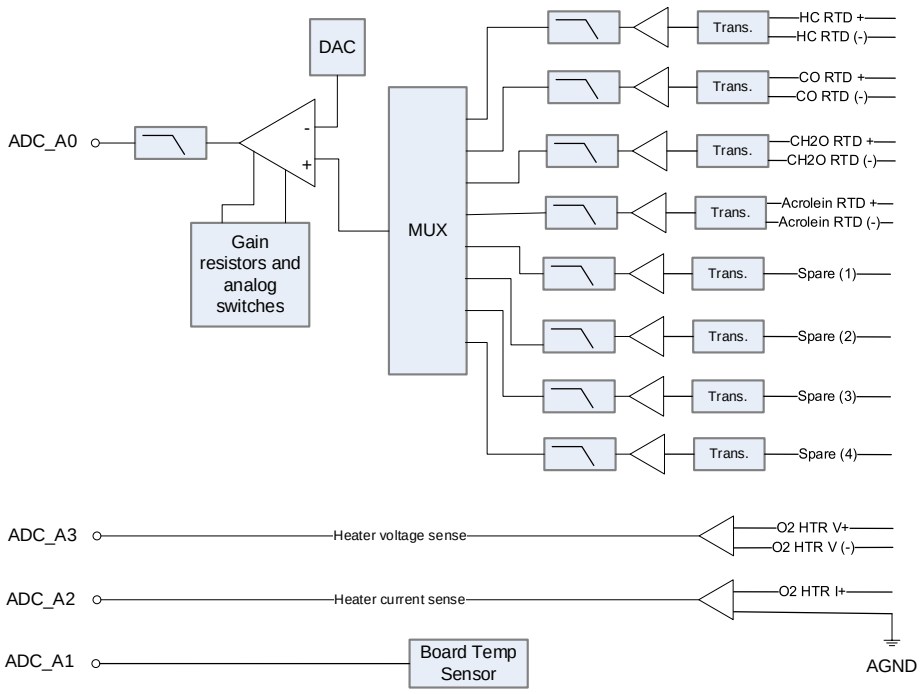

Figure 39. Heater control board signal path.

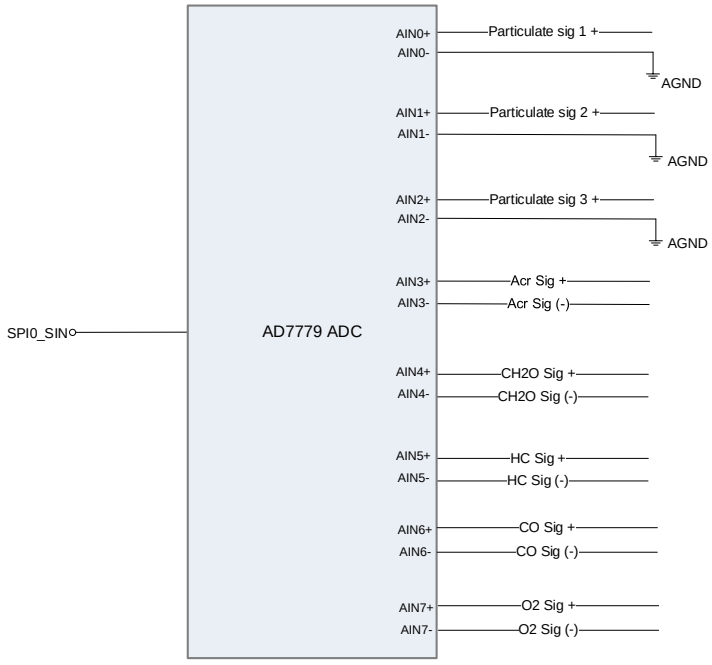

Figure 40. Logger board signal path.

Power Architecture

Power from the battery is delivered into the logger board and then distributed to the heater control board (Figure 41). Each board distributes the power to their respective peripherals and sensors. The 'on' switch for this system is located on the heater control board which means that, although power is being routed through the logger board, power is not be distributed to its peripherals until the switch has been turned on.

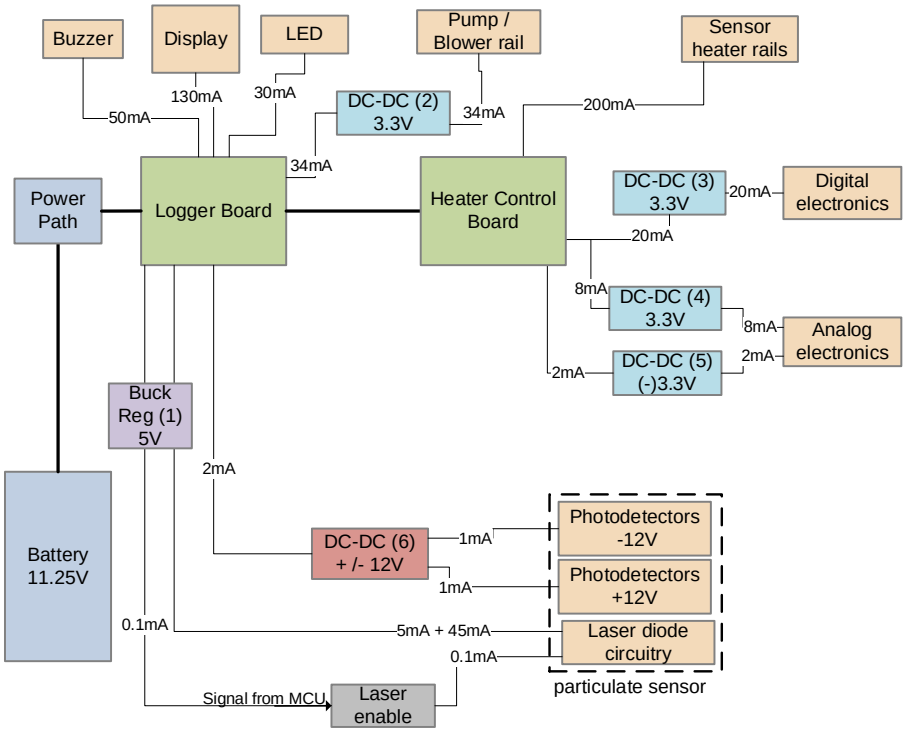

Figure 41. Power architecture.

Power Budget and Battery

Table 3 below shows the power budget for Prototype II. The total current draw of the system is similar to Prototype I as the two additional sensors require relatively low current.

Table 1 Power Budget

Item	Vopr (V)	I @ Vopr (A)	P @ Vopr (W)	Vin (V)	Eff.	I @ Vin (A)	P @ Vin (W)
Display	5	0.14	0.7	11.25	0.8	0.078	0.88
Pump	3.3	0.034	0.11	11.25	0.8	0.012	0.14
MK66 ARM	3.3	0.035	0.12	11.25	0.8	0.013	0.14
AD7779	3.3	0.015	0.050	11.25	0.8	0.055	0.062
O2 Heater	3.2	0.2	0.64	11.25	0.7	0.08	0.91
Acrolein/ Formaldehyde Heater	3.2	0.065	0.21	11.25	0.7	0.026	0.30
HC/ CO Heater	3.2	0.065	0.21	11.25	0.7	0.026	0.30
		0.55	2.0			0.24	2.7

Table 6 has the specifications of the battery in Prototype II and the estimated runtime. Figure 42 shows the battery and the charge gauge on the right side. This allows the user to check the remaining battery without taking it out of the enclosure. Additionally, this battery has female pins that mate with the male pins on the processor and logger board which can be seen in the following section.

Table 6 Battery Specs

Battery	**Vbatt**	**Wh**	**Ah**	**Current**	**Watts**	**Runtime (hr)**	**Dimensions**
Lithium-Ion RRC2040	11.25	33.1875	2.95	0.24	2.7	12.2	3.3” x 2.3” x 0.86”

Figure 42. RRC2040 11.25V battery.

Sensor Manifold

Figure 43 shows the sensor PCB layout to support incorporation of O2, CO, HC, formaldehyde, and acrolein sensors in the manifold. The Acrolein and Formaldehyde sensors share a heater, and the HC and CO sensors share a different heater. Not included in the model is the bond wires that connect the sensors to the surrounding posts, which is then routed on the PCB to the connector.

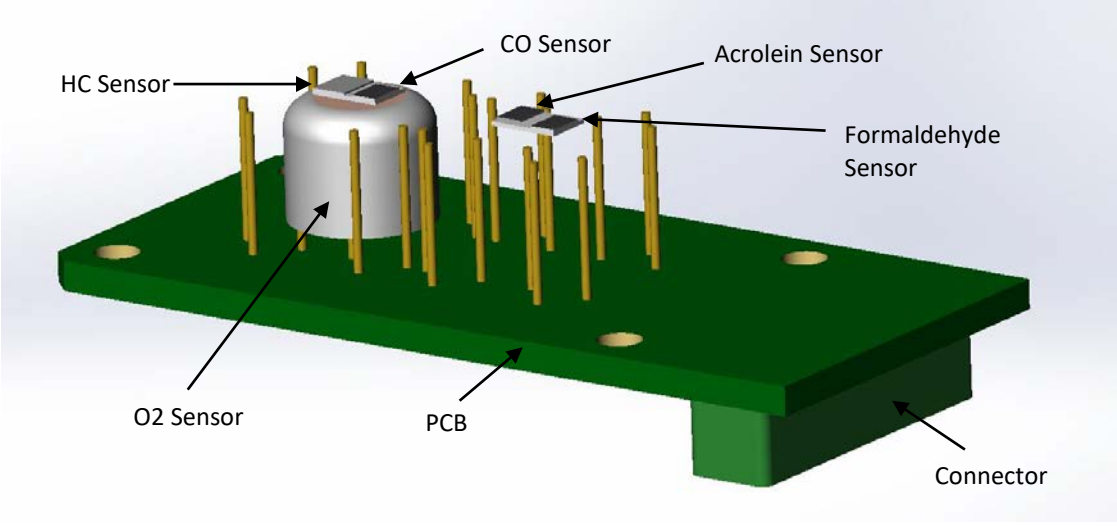

Figure 43. Five sensor board model.

Pump

During Prototype I it was discovered that a pump was necessary to introduce the necessary constant flow to the chemical sensors. The pump for Prototype II is the same pump used and Prototype I and was chosen based on its low voltage requirement, flow ability, and small size (see specs in Table 7). This pump (Figure 44) fits in an envelope approximately 0.5” x 0.9” x 1.2”.

Table 7 Pump Specifications

	Vnom (V)	Current (mA)	Flow (SCCM)	Max Cont. Pressure (psig)
T2-05 Micro Diaphragm Pump	3.3	34	200	2

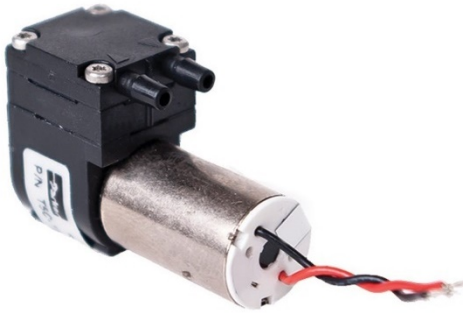

Figure 44. T2-05 pump.

Display and Directional Pad

The display used in Prototype II is approximately half as thick as the display used in Prototype I while maintaining the same screen size. This, along with other changes, will allow the overall size of the system to decrease. Table 8 shows the specs of the new display. Additionally, this display is equipped with an accelerometer enabling screen rotation if the device is rotated.

Table 8 Display Specifications

	Screen Size	Resolution	Interaction	Overall Dimensions
Gen4-uLCD-32PT Display	3.2”	240x320 Backlit	Resistive Touch	2.24” x 3.45” x 0.29”

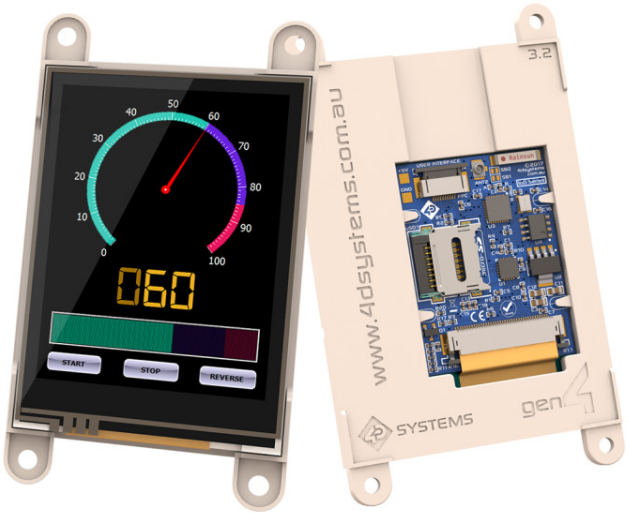

Figure 45. Prototype II display.

System Model

Figure 46 shows the Prototype II components model in exploded view, and approximate configuration used for into the 3D printed housing. Figure 47 shows the prototype as fabricated, indicating the key components. The Prototype II fits and envelope of 8.5” x 1.8”x 4”, with a portion or reduced width to facilitate holding the unit.

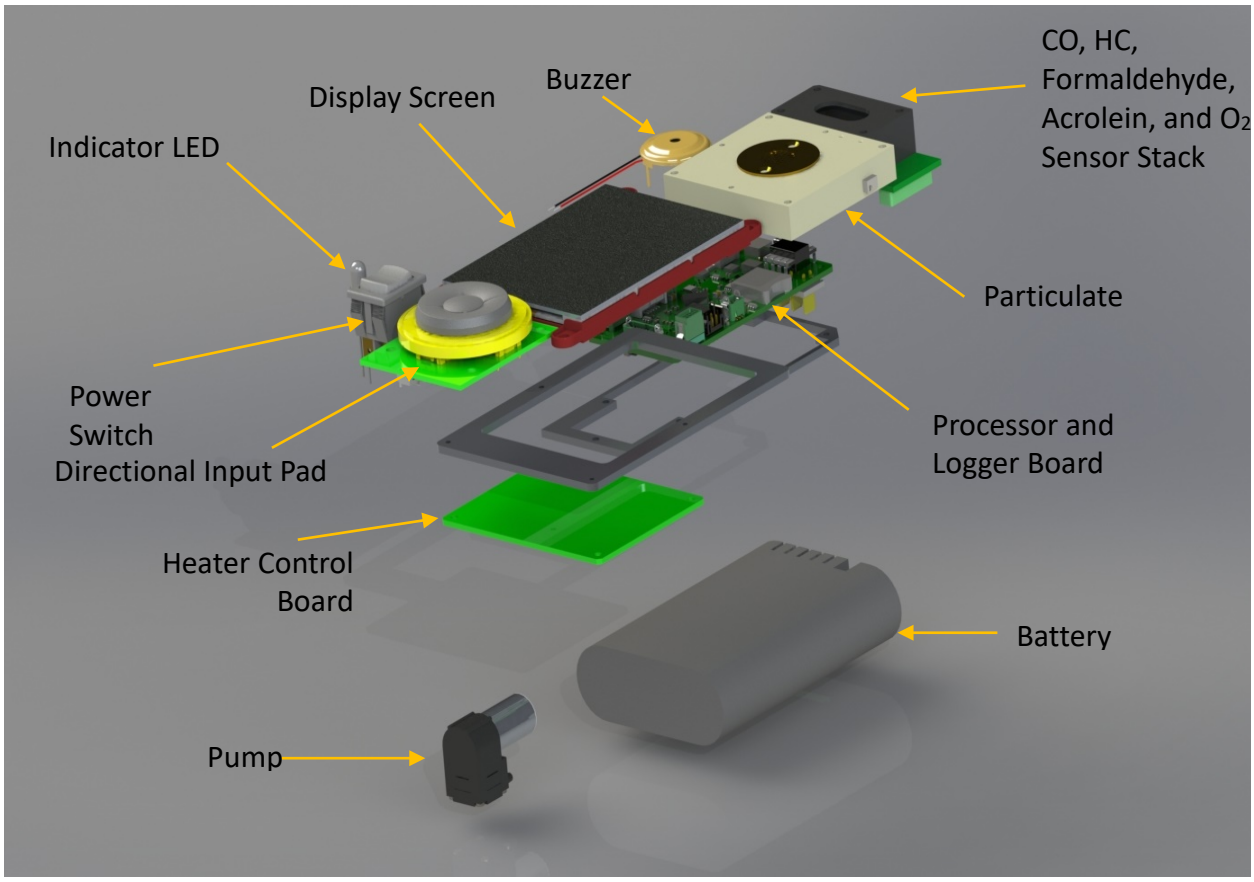

Figure 46. Prototype II test integration exploded view.

Figure 47. Prototype II as fabricated.

7. SMOKE CHARACTERIZATION

7.1 Preliminary Study

The initial testing of the particulate and micro-fabricated gas sensors, prior to the miniaturization, have been conducted during the preliminary study in a controlled burn mode in the burn room at the Fire Training Academy of the Cleveland Division of Fire (Fig. 48). Selected results have been published [Takahashi et al., 2014].

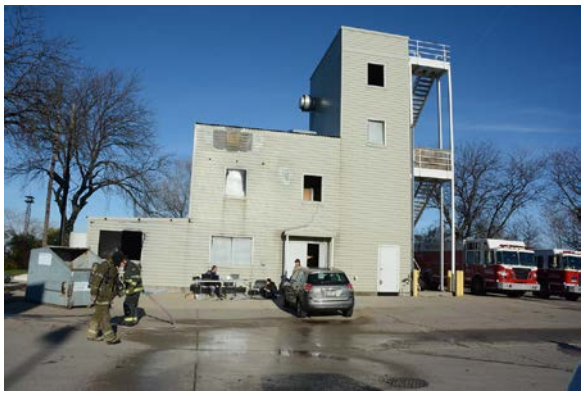

Figure 48. Burn building at Cleveland Fire Training Academy.

Fuels are (1) wooden pallets, (2) a mattress, or (3) a couch without cushions placed in the center of a closed burn room (21 ft. length × 13 ft. width × 8½ ft. height). Two gas sampling tubes, a heat flux transducer, and five K-type thermocouple are installed on a sensor stand (Fig. 49) approximately 1.5 m away from the fire source.

Figure 49. Sensor stand.

The gas sampling tube is connected to the MPASS particulate sensor and in tandem a tapered element oscillating microbalance (TEOM) personal dust monitor (Thermo Science PDM3600). Another tube is connected to an array of the micro-fabricated gas sensors for O_2, CO, CO_2, and hydrocarbons. The real-time data are acquired throughout the ignition, burning, extinguishment, and post-fire periods using laptop computers.

Test 1

Figure 50 shows photographs of Test 1 setup for wood pallets and straw before and after the burn. The fuel burned down almost completely during a burn period (approximately 12 minutes).

(a) (b)

Figure 50. Photographs of wood pallets and straw: (a) before and (b) after the burn (Test 1).

Figure 51 shows the measured heat flux and temperature at various heights (z) from the floor. At z = 1.52 m, they peaked are 8 kW/m^2 and 250 °C, respectively, at ≈1 minute after ignition and decreased rapidly as water was sprayed over the fire at ≈11 min. after ignition. The heat flux trace correlated closely that of the temperature. Figure 52 shows the measured concentrations of gases (O_2, CO, CO_2, and hydrocarbons). The hydrocarbon and CO concentration increased rapidly and reached the maximum ranges, i.e., the signals saturated at 8000 ppm and 20000 ppm, respectively. The O_2 concentration decreased down to the minimum of ≈14 %, while the CO_2 concentration maintained a high level of ≈6 %. Although the MPASS and TEOM dust monitor measurements were attempted for Test 1 (not shown), the MPASS signal saturated (5 V) and a filter for the TEOM unit exceeded the allowable pressure drop due to clogging almost immediately after smoke was first detected. Apparently, too much smoke was generated for the highly sensitive instruments.

Test 2

Figure 53 shows a photograph of Test 2 setup for a mattress on wood pallets and straw before the burn. The fuel burned down completely (not shown), leaving metal wires and springs, during a burn period (approximately 10 minutes). Figure 54 shows the measured heat flux and temperature. At z = 1.52 m, they peaked are 9 kW/m^2 and 280 °C, respectively, at ≈4 minutes

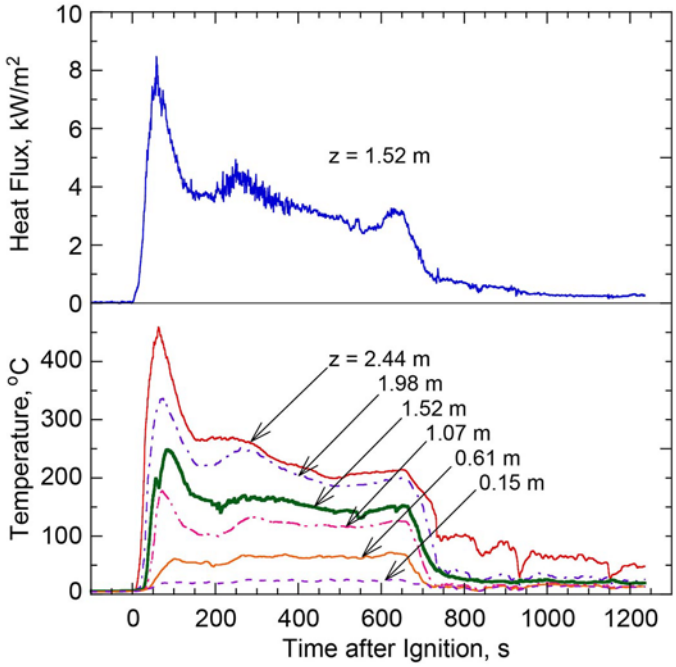

Figure 51. Measured heat flux and temperature (Test 1).

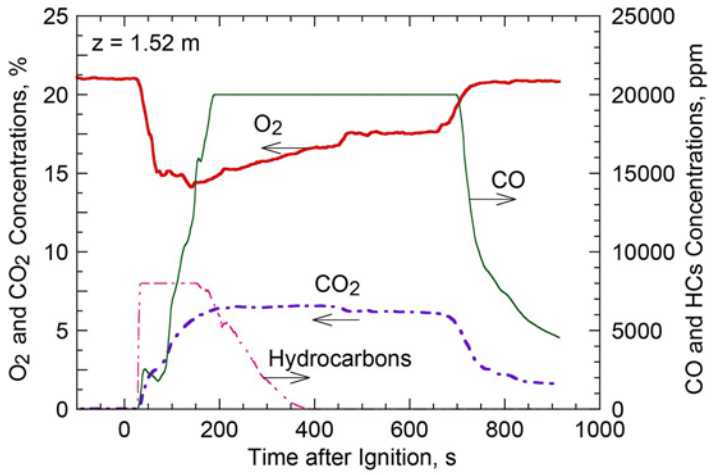

Figure 52. Measured concentrations of O_2, CO, CO_2, and hydrocarbons (Test 1).

Figure 53. Photographs of a mattress on wood pallets and straw before the burn (Test 2).

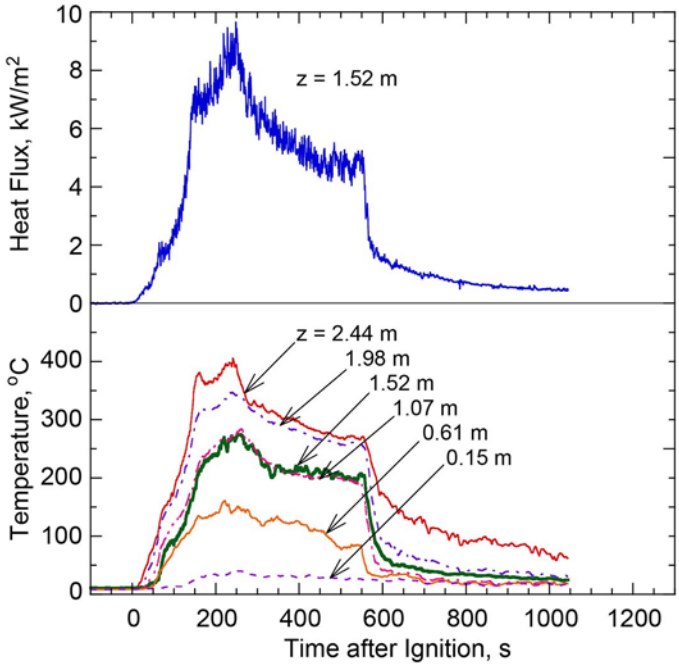

Figure 54. Measured heat flux and temperature (Test 2).

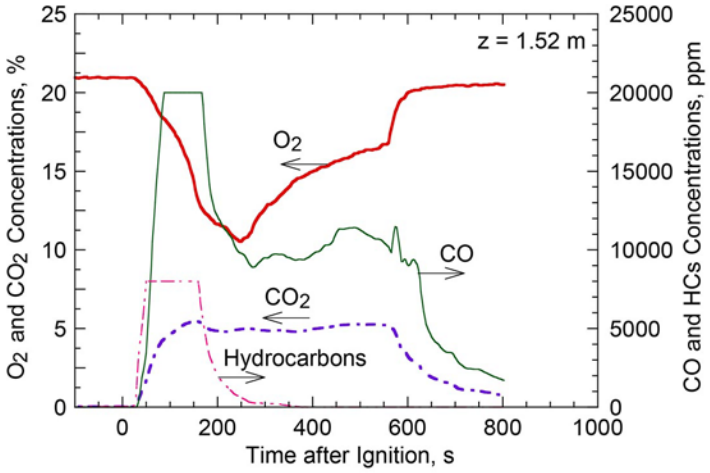

Figure 55. Measured concentrations of O_2, CO, CO_2, and hydrocarbons (Test 2).

after ignition and decreased rapidly as water was sprayed over the fire at ≈10 min. after ignition. Figure 55 shows the measured concentrations of gases (O_2, CO, CO_2, and hydrocarbons). The hydrocarbon and CO concentration increased rapidly and reached the maximum ranges, but the CO signal came down at ≈3 min and maintained at a 10000 ppm-level. The O_2 concentration decreased to a minimum of ≈10 %, while the CO_2 concentration maintained a high level of ≈5 %.

Figure 56 shows the measured MPASS signals and TEOM mass concentration at z = 1.52 m. The abscissa is arbitrary time, instead of the time from ignition. The MPASS's Channel 1 signal (blue) represents the surface area and Channel 2 signal (green) indicates the mass concentration (Fig. 56a). Both signals saturated (≈5 V), but the Ch. 2 signal came down during the burn and showed a good correlation with the mass concentration measure by the TEOM dust monitor. Thus, by scaling the MPASS Ch. 2 signal, two curves coincide each other fairly well as shown in

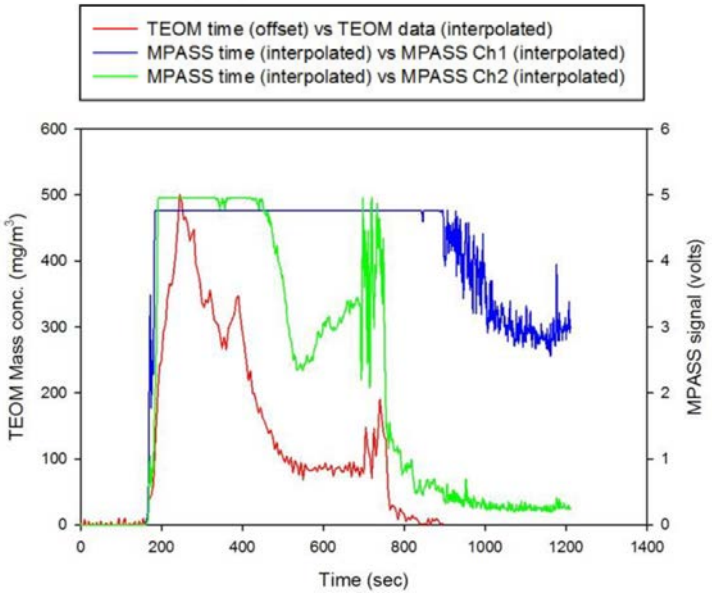

(a)

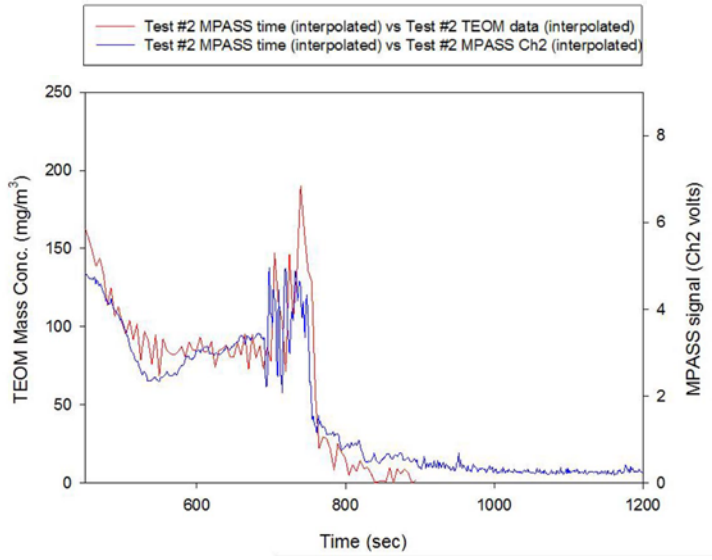

(b)

Figure 56. TEOM mass concentration, (a) measured MPASS signals, and (b) adjusted MPASS Ch.2 signal at z = 1.52 m (Test 2).

Fig. 56b. This result indicates that the MPASS can be used for the mass concentration measurement for the smoke generated by wood burning with a proper calibration.

Test 3

Figure 57 shows photographs of Test 3 setup for a couch without cushions before and after the burn. The fuel burned down except for a wood frame during a burn period (approximately 10 minutes). Figure 58 shows the heat flux and temperature at the height. At z = 1.52 m, they reached peaks of ≈9 kW/m^2 and 250 °C, respectively, at ≈3 min. after ignition and decreased rapidly as water was sprayed over the fire at ≈10 min. after ignition. Figure 14 shows the

(a) (b)

Figure 57. Photographs of a couch without cushions: (a) before and (b) after the burn (Test 3).

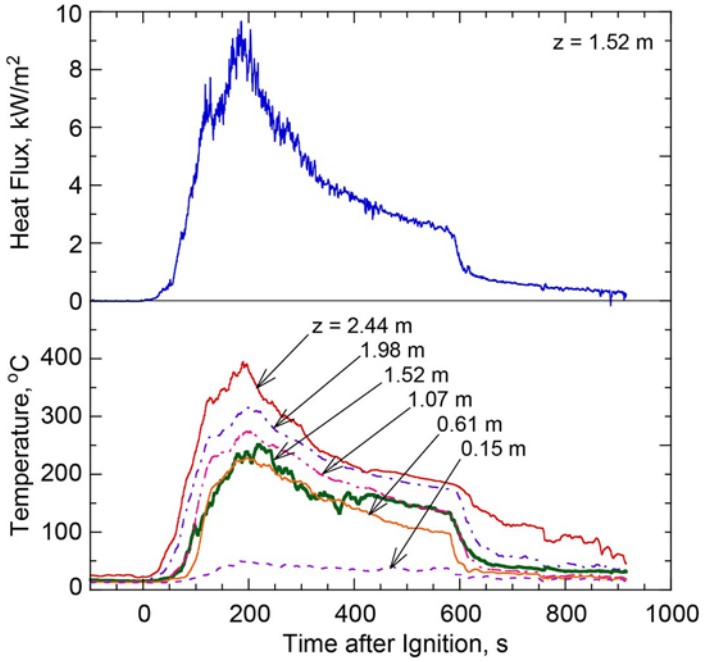

Figure 58. Measured heat flux and temperature (Test 3).

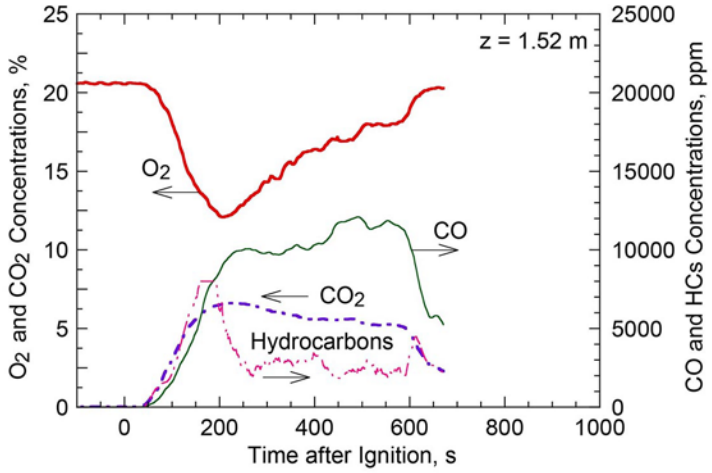

Figure 59. Measured concentrations of O_2, CO, CO_2, and hydrocarbons (Test 3).

measured concentrations of gases (O_2, CO, CO_2, and hydrocarbons). The hydrocarbon and CO_2 concentration peaks as well as the minimum O_2 concentration point approximately coincided with the heat flux and temperature peaks, while the CO concentration maintained high levels. Figure 59 shows the measured MPASS signals and TEOM mass concentration at z = 1.52 m. The TEOM dust monitor signal (red curve in Fig. 59) exceeded significantly the device's measurement range (200 mg/m^3). The MPASS signal variations for total aerosolized mass (ch.2, green) follows the TEOM output qualitatively, while the signal for surface area (Ch. 1, blue) saturated most of the time due to excessive particulate loading in the environment. Although further testing is desirable to simulate post-fire environments with low concentration levels, the sensitivities of the MPASS and gas sensors are verified to be adequate.

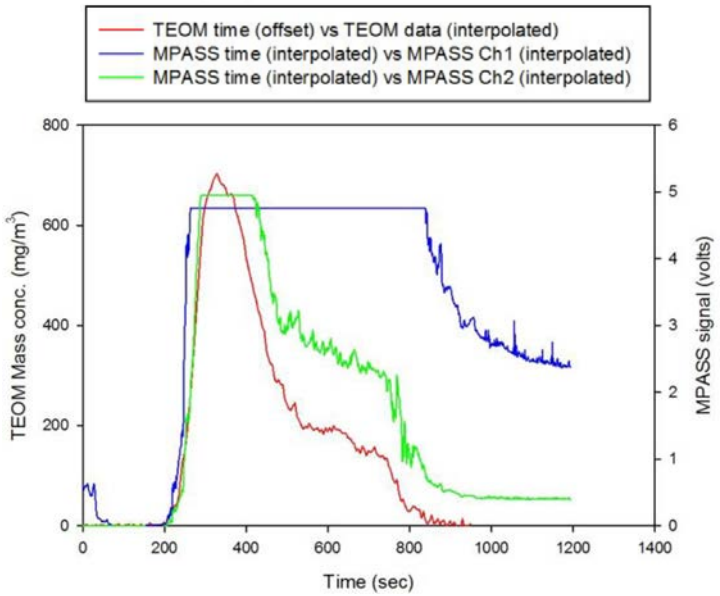

(a)

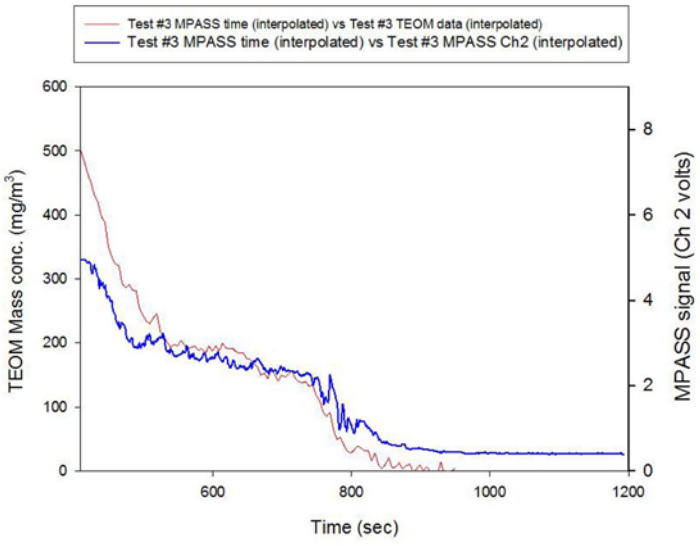

(b)

Figure 59. TEOM mass concentration, (a) measured MPASS signals, and (b) adjusted MPASS Ch.2 signal at z = 1.52 m (Test 3).

In addition to the burn-room testing, small smoke chamber tests were conducted on the MPASS and micro-fabricated gas sensors at the NASA's Gases & Aerosol from Smoldering Polymers (GASP) facility (Fig. 60) [53]. The entire GASP facility is contained in polycarbonate boxes attached to lab ventilation for safe operation. Smoke containing aerosol particles and gases are generated by thermal decomposition and oxidation of wood samples (from the wood pallet used for the field fire testing) inside a tube furnace at 250 °C, 300 °C, 350 °C, 400 °C. Filtered air is flowed through the furnace to push the decomposition byproducts into a smoke chamber (29" W x 23" D x 30" H, 326 L). The smoke chamber includes pass-through for smoke/byproduct inlet, gas outlets to some of the analytical instruments. The laboratory is equipped with a variety of instruments; e.g., particulate analyzers, Fourier transform infrared spectrometer (FTIR), and gas chromatographs, etc. In this study, the TEOM dust monitor, Ultrafine Condensation Particle Counter (UCPC, TSI 3776) equipped with an Electrostatic Classifier (TSI 3080), and a laser-based CO multipass analyzer (Vista Photonics COMA). Figures 61 and 62 show examples of the outputs from the UCPC and thermogravimetric analysis (TGA).

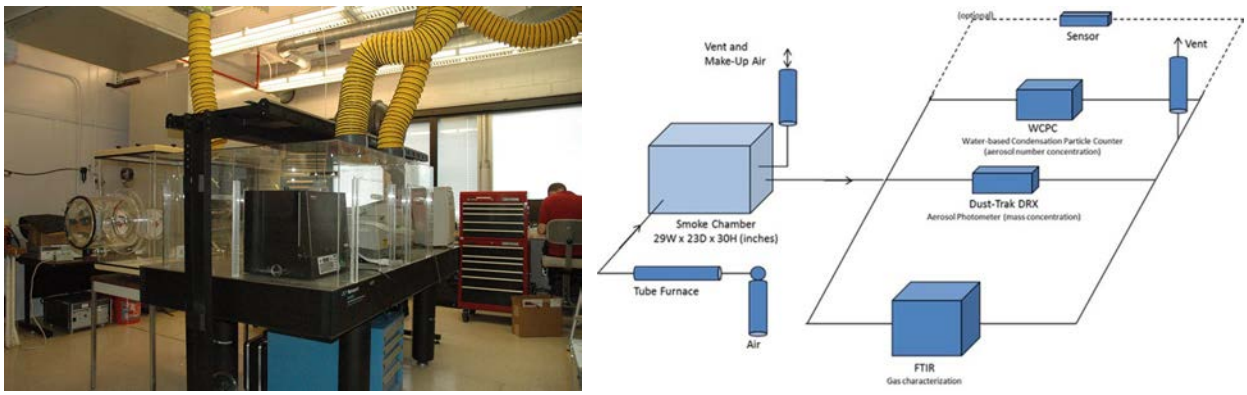

(a) (b)

Figure 60. NASA Gases & Aerosol from Smoldering Polymers (GASP) facility: (a) photograph and (b) flow diagram.

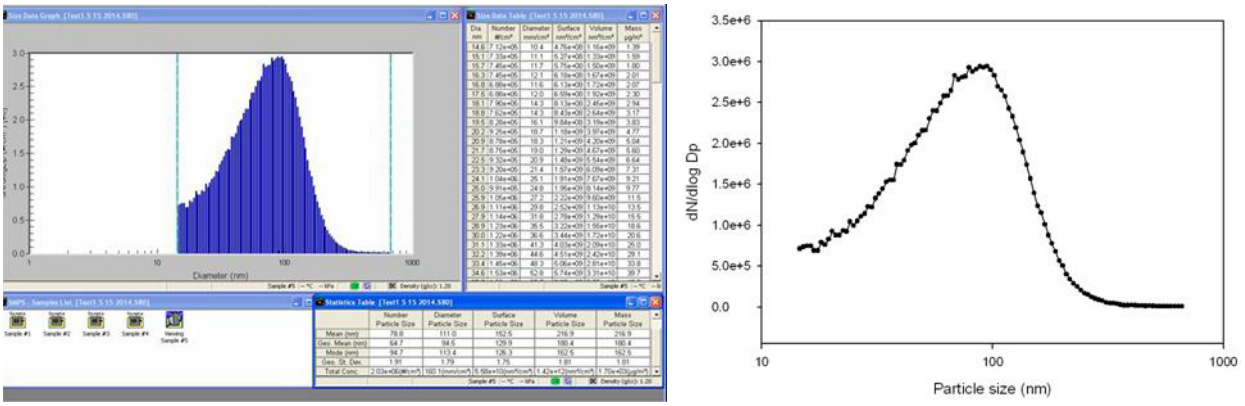

(a) (b)

Figure 61. Ultrafine Condensation Particle Counter (UCPC) signals: (a) screen shot and (b) particle size distribution for a wood sample.

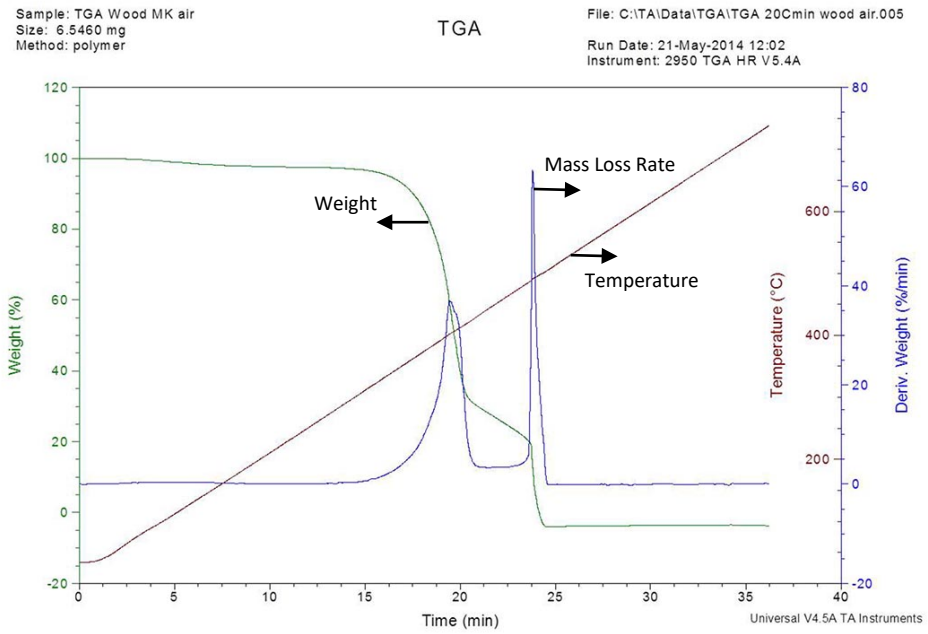

Figure 62. Thermogravimetric analysis (TGA) of a wood sample.

7.2 Laboratory Experiments

To characterize the effluents of pyrolysis or burning from materials, the concentration measurements of particulates and toxic gases were made using the standard fire testing equipment in the UL Fire and Combustion Laboratories at Case Western Reserve University. The results of the studies were presented at technical conferences and culminated in M.S. theses [Matsuyama, 2019; Wen, 2019; Tian, 2019]. The abstracts of the theses are as follows.

Toxic gas and particulates characterization in a smoke density chamber [Matsuyama, 2019]

Smoke and toxic gas inhalation is a major cause of civilian and firefighter deaths during a fire incident. Real-time measurements of the concentrations of particulates and toxic gases in a smoke density chamber (SDC) have been made using a tapered element oscillating microbalance (TEOM) dust monitor, a Fourier transform infrared (FTIR) gas analyzer, and a hand-held particulate/gas sensor prototype (O_2, CO, and hydrocarbons) under development (Fig. 63). The FTIR analyzes a total of 21 toxic gases, including both asphyxiants (CO, HCN, etc.) and irritants (HCl, HBr, acrolein, formaldehyde, etc.). Common building materials, plastics, and selected woods at various moisture contents are used as the fuel. A specimen is placed vertically or horizontally and heated with an incident radiant flux of 25 kW/m^2 under a flaming or non-flaming condition. The smoke obscurity and the particulate mass concentration correlate well with live readings of the CO concentration. The prototype device for fire service is being validated by the standard analytical equipment (TEOM and FTIR).

The initial testing of Prototype I (Fig. 64) was conducted in the smoke density chamber using wood (pine) as the fuel. Because the CO concentration in SDC, even when using a non-standard small specimen size (25mm × 25mm × 6.35mm thickness), was much higher than the maximum range for Prototype I (100 ppm), the reading saturated in a short time (≈5 min).

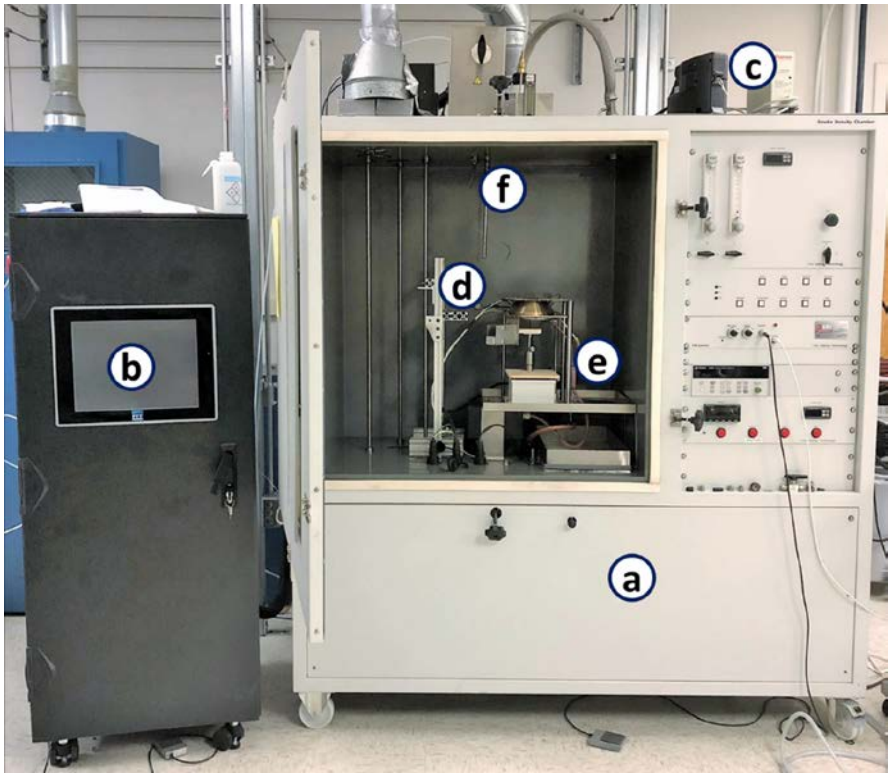

Figure 63. Experiment apparatus. (a) Smoke density chamber, (b) FTIR gas analyzer, (c) TEOM dust monitor, (d) bracket for hand-held prototype sensor, (e) ISO 5659 cone setup, and (f) sampling ports for FTIR and TEOM. The smoke density measurement is taken using a light-beam transmittance placed in the back-left corner of the chamber, between the three poles pictured left of (d).

Figure 64. A hand-held particulate and toxic-gas sensor device (Prototype I).

The gas mixtures were also sampled in inflating sample bags and analyzed by a GC-MS (Perkin Elmer Torion T-9) at the NASA Glenn Research Center for the gaseous species between 41-500 amu.

A laboratory scale study of particulates generation from charring and non-charring polymers [Wen, 2019]

Polymers have been widely used in the contemporary age. However, the nature of polymers makes them dangerous fuel sources. For decades, studies have focused on polymers' heat release rates and largely neglected smoke toxicity. Additionally, soot particles may result in permanent and chronic harm to human bodies, such as lung and skin cancers. The primary goal of this study is to gain a better understanding of the particulate generation and other combustion characteristics of representative non-charring and charring polymers; i.e., polymethylmethacrylate (PMMA) and polyvinyl chloride (PVC), respectively. A standard cone calorimeter (Fig. 64) is used to collect and analyze particulate-laden gas mixtures from the exhaust flow. Polymer specimens with varied thicknesses are tested under various irradiance. Measurements include the rates of heat release, mass loss, and smoke production, the yields of CO, CO_2, and O_2, and the soot characteristics. Non-charring PMMA burns well and cleanly. By contrast, charring PVC demonstrates distinctively higher particulate/smoke and CO production (i.e., lower combustion efficiency), lower heat-release rates, and longer times to ignition. Therefore, the desirable fire safety nature of the charring polymer is achieved by the lower flammability but, in exchange, it results in higher toxicity.

Figure 64. Cone calorimeter.

A study of charring behavior of woods based on internal temperature and CT-scan measurements [Tian, 2019]

Recent trends of increasingly tall wood buildings call for further research on the combustion and carbonization of wood. Burning, charring, and smoke characteristics of two common building woods (pine and oak) with different thicknesses (6.35 to 38.1 mm) and moisture contents (0 to 40 %) were investigated in a cone calorimeter under different incident radiant fluxes (25, 35, and 50 kW/m^2). Besides the standard cone calorimeter outputs (the heat release rate, time to ignition, and the concentrations of O_2, CO, CO_2, and smoke), real-time temperature variations in the interior of the specimens were measured by six thermocouples embedded at different depths. The charring rate of the wood was determined by tracking the time when each thermocouple reached 300 ℃. The heat-release rate curve exhibited two peaks at the initial and last flares and a reduced-level charring period in-between, typical of wood burning. The second heat-release rate peak was initiated (abruptly for pine) when the charring wave reached the back side of the wood specimen. Furthermore, computed tomography (CT)-scanning of the specimens (Fig. 65), quenched at different times after ignition, revealed the internal structure and yielded the charring rate independently, which was consistent with that obtained from the temperature measurement. With an aim at reducing the risk of fire, this study demonstrates the laboratory-scale methods useful to understand the physical processes taking place in the interior of wood specimens and how they relate to the various burning characteristics of woods.

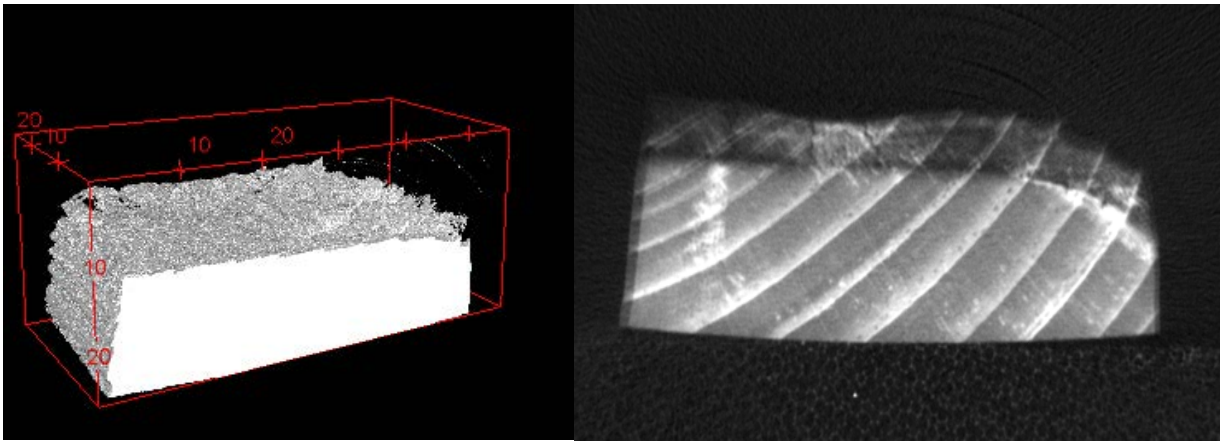

(a) (b)

Figure 65. (a) A reconstructed CT-scanned image of wood with char removed and (b) a tomographic section of the scanned sample.

7.3 Field Fire Experiments

The first unit of Prototype I hand-held detector was tested briefly in a wildland fire in northern California in August 2019 by the US Forest Service (George Broyles, stationed in Boise, Idaho). Although it was a great opportunity to test the prototype in a real wildfire, there was not sufficient time for us to prepare for the unit due to such an urgent call for the Forrest Service mission. Nevertheless, we were able to obtain valuable feedback about the sensors' signal stability and saturation issues from the first field fire test user.

The second unit of the Prototype I was fabricated with improvements based on the testing results of the first unit of the Prototype-1. The improvements include:

- Zeroed and reset the baseline by averaging offset values during the initialization and heater warm-up period (~8 min).
- Increased (temporarily) the full scale of the CO sensor from 100 ppm to 5000 ppm to cover high concentrations potentially encounter in real fires and in the laboratory testing.
- Made minor changes in the design of the 3D printed container, including a recessed ON/OFF switch, sensors and pump locations, and the container overall size.

7.4 Future Research Proposal

The Schottky-diode SiC-based acrolein and formaldehyde sensors were used in the Prototype II device mainly because of the simplicity of the associated electronics. Further testing of Prototype II in the laboratories and in real fires must be conducted in order to improve and implement the technology into a marketable product in the future. Furthermore, the membrane-electrolyte acrolein and formaldehyde sensors should also be studied to incubate the emerging technology.

8. SUMMARY

For firefighter health and safety, there is a need for hand-held detectors capable to measure the real-time concentrations of particulates and toxic-gases simultaneously, particularly during the post-fire period.

Two types of micro-fabricated sensors for detecting sensory irritant gases, i.e., acrolein and formaldehyde, were studied, while the NASA-developed multi-parameter aerosol scattering sensor was miniaturized further. The particulate and gas sensors, together with the control electronics, were integrated into two prototypes consecutively. The Prototype I unit included the sensors for particulate, low-level CO, O_2, and hydrocarbon sensors, and Prototype II for particulate, high-level CO, O_2, hydrocarbon, acrolein, and formaldehyde.

To gain basic knowledge of the smoke generation and toxicity characteristics, the pyrolizing or flaming wood materials were studied using the smoke density chamber and the cone calorimeter. Main findings include: (1) the non-flaming pyrolysis of wood generated much more (~3×) CO than the flaming condition, (2) the formaldehyde concentration was an order of magnitude higher than acrolein, and (3) both formaldehyde and acrolein concentrations were correlated well with the CO concentration. The results were informative for the device development.

In addition to initial laboratory testing of the prototypes, a brief attempt was made to test the first Prototype I unit in the wildland fire in California by the USDA Forest Service. Further field fire testing and debugging efforts are needed for Prototype II to implement the technology into a commercial product in the future.

ACKNOWLEDGEMENT

The research team would like to thank contributions by the fire-related organization Project Partners and the Project Technical Panel members. Assistance in conducting experiments by graduate and undergraduate students (CWRU), George Broyles (USDA Forest Service), Morgan Miller (Leidos at NASA Glenn), Batt. Chief (ret.) Sean DeCrane, and Capt. Roy Ziganti, Jr. (Cleveland Division of Fire) is acknowledged.

PUBLICATIONS

1. Takahashi, F., Greenberg, P., Hunter, Firefighter particulate and gas sensor technology, *Fire Safety (FS)-World*, Fall edition, 2014.

2. Matsuyama Y., and Takahashi F., Effects of surface orientation on the smoke toxicity of flaming and pyrolyzing wood, *Fire Safety Journal*, 2019 (under review).

PRESENTATIONS

3. Takahashi, F., Greenberg, P., Hunter, G., Grant, C., Development of fire fighter particulate and gas sensor technology, NFPA Conference & Expo, Las Vegas, NV, June 9-12, 2014.

4. Takahashi, F., Greenberg, P., Hunter, Firefighter particulate and gas sensor technology, *Fire Safety (FS)-World*, Fall edition, 2014.

5. Takahashi, F., Liu, C.C., Greenberg, P.S., Hunter, G.W., Kulis, M.J., Carranza, S., Makel, D.B., Broyles, G., DeCrane, S. Grant, C.C., Ranganathan, S., Development of real-time particulate and toxic-gas sensors for firefighters, 5th International Fire Behavior and Fuels Conference, Portland, OR, April 11-15, 2016.

6. Takahashi, F., Liu, C.C., Greenberg, P.S., Hunter, G.W., Kulis, M.J., Carranza, S., Makel, D.B., Real-time particulate and toxic-gas sensors for firefighters, Poster session at the Eighth International Seminar on Fire & Explosion Hazards (ISFEH8), Hefei, China, April 25-28, 2016.

7. Takahashi, F., Liu, C.C., Greenberg, P.S., Hunter, G.W., Kulis, M.J., Carranza, S., Makel, D.B., Real-time particulate and toxic-gas sensors for firefighters, American Industrial Hygiene Conference & Exposition (AIHce), Baltimore, MD, May 21-26, 2016.

8. Takahashi, F., Liu, C.C., Greenberg, P.S., Carranza, S., Hunter, G.W., Kulis, M.J., Berger, G., Real-time measurements of particulate and toxic-gas concentrations, 15th International Conference on Fire and Materials, San Francisco, February 6-8, 2017.

9. Takahashi, F., Liu, C.C., Greenberg, P.S., Hunter, G.W., Kulis, M.J., Berger, G., Xu, J., Carranza, S., Williams, J., Makel, D.B., Particulates and toxic-gas sensors for firefighters, Poster session at the 10th U. S. National Combustion Meeting of the Combustion Institute, College Park, MD, April 23-26, 2017.

10. Takahashi, F., Liu, C.C., Greenberg, P.S., Hunter, G.W., Kulis, M.J., Berger, G., Xu, J., Carranza, S., Williams, J., Makel, D.B., Particulates and toxic-gas sensors for firefighters, Poster session at the 12th International Symposium on Fire Safety Science, Lund University, Sweden, June 12-16, 2017.

11. Matsuyama, Y., Takahashi, F., Smoke toxicity measurements in a smoke density chamber Spring Technical Meeting of the Central States Section of The Combustion Institute, Minneapolis, MN, May 20-22, 2018.

12. Tian, Y., Kang, J., Takahashi, F., Effects of moisture content on burning characteristics of woods in a cone calorimeter, Spring Technical Meeting of the Central States Section of The Combustion Institute, Minneapolis, MN, May 20-22, 2018.

13. Matsuyama, Y., Takahashi, F., Particulates and toxic-gas measurements in a smoke density chamber, Poster session at the Thirty-Seventh International Symposium on Combustion, Dublin, Ireland, July 29-August 3, 2018.
14. Matsuyama Y., and Takahashi F., Toxic Gas and particulate characterization in a smoke density chamber, 9th International Seminar on Fire and Explosion Hazards (ISFEH), St. Petersburg, Russia, April 21−26, 2019.
15. Tian, Y., Kang, J., Takahashi, F., Effects of moisture content on burning behavior of woods in a cone calorimeter, 12th The Asia-Pacific Conference on Combustion (ASPACC), Fukuoka, Japan, July 1-5, 2019.

THESES

1. Matsuyama, Y., Toxic gas and particulates characterization in a smoke density chamber. M.S. Thesis, Case Western Reserve University, May 2019.
2. Wen, C., A laboratory scale study of particulates generation from charring and non-charring polymers. M.S. Thesis, Case Western Reserve University, May 2019.
3. Tian, Y., A study of charring behavior of woods based on internal temperature and CT-scan measurements. M.S. Thesis, Case Western Reserve University, May 2019.

REFERENCES

Alarie, Y. (1985). The toxicity of smoke from polymeric materials during thermal decomposition. Am. Rev. Pharmacol. Toxicol. 25, 325-347.

Alarie, Y. (2002). Toxicity of Fire Smoke. Crit. Rev. Toxicology, 32, 259-289.

Anon. (2006). TLVs and BEIs Based on the Documentation of the Threshold Limit Values for Chemical Substances and Physical Agents & Biological exposure Indices, American Conference of Governmental Industrial Hygienists (ACGIH).

Anon. (2011). Report of the 2nd National Fire Service Research Agenda Symposium, National Fire Academy, May 20 - 22, National Fallen Firefighters Foundation (NFFF), p. 50.

Anon. (2013). National Occupational Research Agenda (NORA), National Public Safety Agenda for Occupational Safety and Health Research and Practice in the U.S. Public Safety Sector, 29 Oct. 2013 Revision.

Anon. (2014). Documentation for Immediately Dangerous to Life or Health Concentrations (IDLHs), National Institute for Occupational Safety and Health (NIOSH). http://www.cdc.gov/niosh/idlh/default.html.

Cumpston, K.L., Rose, S.R. (2017). Carbon Monoxide: The Other Silent Killer. Emergency Medicine. November; 49 (11):486-497. https://www.mdedge.com/emergencymedicine/article/151600/toxicology/carbon-monoxide-other-silent-killer.

Auel, R.M. et al. (1987). US Patent #4,692,220 issued September 8.

Bagotzky, V.S., Vasilyev, Y.B. **(**1964). Some characteristics of oxidation reactions of organic compounds on platinum electrodes. Electrochimica Acta 9, 869-882.

Bauer, G.L., and Ginbel, R.A. (2004). Smoke Inhalation Injury. In *Medical Toxicology* (Eds., Dart, R.C. Caravati, E.M., McGuigan, M.A.), 3rd ed., Lippincott Williams & Wilkins, Philadelphia, PA, 2004, pp. 1203-1210.

Baxter, C.S., Ross, C.S., Fabian, T., Borgerson, J.L., Shawon, J., Gandhi, P.D., Dalton, J.M., Lockey, J.E. (2010). Ultrafine Particle Exposure During Fire Suppression, Journal of Occupational & Environmental Medicine, 52: 791-796.

Birky, M.M., and Clarke, F.B. (1981). Inhalation of toxic products from fires. Bull. N.Y. Academic Med., 57, 997-1013.

Bolstad-Johnson, D.M., Burgess, J.L., Crutchfield, C.D., Storment, S., Gerkin, R., Wilson, J.R. (2000). Characterization of Firefighter Exposure during Fire Overhaul, American Industrial Hygiene Association Journal, 61: 636-641.

Bowes, P.C. (1974). Smoke and Toxicity Hazards of Plastics in Fires. Ann, Occup. Hygine, 17, 143-157.

Brandt-Raul, P.W., Fallon, Jr., L.F., Tarantini, T., Idema, C., Andrews, L. (1988). Health hazards of fire fighters: exposure assessment. British Journal of Industrial Medicine, 45, 606-612.

Breen, P.H., Isserles, S.A., Westley, J., Roizen, M.F., Taitelman, U.Z. (1995). Combined carbon monoxide and cyanide poisoning: a place for treatment? Anesth. Analg., 80, 671-677.

Bryant, R.A., Butler, K.M., Vettori, R.L., Greenberg, P.S. (2007). Real-time particulate monitoring—detecting respiratory threats for first responders: workshop proceedings, NIST Special Publication 1051, National Institute of Standards and Technology, December.

Burgess, J.L., Nanson, C.J., Bolstad-Johnson, D.M., Gerkin, R., Hysong, T.A., Lantz, R.C., Sherrill, D.L., Crutchfield, C.D., Quan, S.F., Bernard, A.M., Witten, M.L. (2001). Adverse Respiratory Effects Following Overhaul in Firefighters, Journal of Occupational and Environmental Medicine, 43: 467-473.

Chung, P. R. et al. (2013). Formaldehyde gas sensors: a review. Sensors 13, 4468-4484.

Fahy, R.F., LeBlanc, P.R., Molis, J.L. (2018). Firefighter Fatalities in the United States-2017. National Fire Protection Association, Quincy, MA, June. Available at https://www.nfpa.org/News-and-Research/Data-research-and-tools/Emergency-Responders/Firefighter-fatalities-in-the-United-States [Verified 10 June 2019].

Fahy, R.F. (2010). U.S. Fire Service Fatalities in Structure Fires, 1977-2009, National Fire Protection Association, Quincy, MA, June.

Geibe, J.R., Holder, J., Peeples, L., Kinney, A.M., Burress, J.W., Kales, S.N. (2008). Predictors of on-duty coronary events in male firefighters in the United States. Am. J. Cardiol., 101, 585.

Gold, A., Burgess, W.A., Clougherty, E.V. (1978). Exposure of firefighters to toxic air contaminants. Am. Ind. Hyg. Assoc, J., 39, 534-539.

Gold, D.R., Litonjua, A.A., Zanobetti, A., Coull, B.A., Schwartz, J., MacCallum, G., Verrier, R.L., Nearing, B.D., Canner, M.J., Suh, H., Stone, P.H. (2005). Air pollution and ST-segment depression in elderly subjects. Environ. Health Perspect., 113, 883–887.

Gong, H., Jr., Linn, W.S., Clark, K.W., Anderson, K.R., Sioutas, C., Alexis, N.E., Cascio, W.E., Devlin, R.B. (2008). Exposures of healthy and asthmatic volunteers to concentrated ambient ultrafine particles in Los Angeles. Inhal. Toxicol., 20, 533-45.

Grant, C.C. (2007). Respiratory exposure study for fire fighters and other emergency responders, Fire Protection Research Foundation, December.

Hall, A.H., and Schnepp, R. (2011). Cyanide: Fire Smoke's Other "Toxic Twin". Fire Engineering, December 1, 2011.

Hartzell, G.E., (1996). Overview of combustion toxicology. Toxicology, 115, 7-23.

Holder, J.D., Stallings, L.A., Peeples, L., Burress, J.W., Kales, S.N. (2006). Firefighter heart presumption retirements in Massachusetts 1997-2004. J. Occup. Environ. *Med.*, 48, 1047-53.

Howe, L.H. (1976). Voltammetric determination of acrolein. EPA-600/7-76.005, July.

Hunter, G.W., Xu, J.C., and Lukco, D. (2008a). US Patent 7,389,675B1.

Hunter, G.W., Xu, J.C., Dungan, L.K., Ward, B.J., Rowe, S., Williams, J., Makel, D.B., Liu, C.C., and Chang, C.W. (2008b). Smart Sensor Systems for Aerospace Applications: From Sensor Development to Application. ECS Transactions, 16 (11) 333-344.

Hunter, G.W. et al. (2010). Smart sensor systems. The Electrochemical Society Interface, winter 29-34.

Ibald-Mulli, A., Timonen, K.L., Peters, A., Heinrich, J., Wölke, G., Lanki, T., Buzorius, G., Kreyling, W.G, de Hartog, J., Hoek, G., ten Brink, H.M., Pekkanen, J. (2004). Effects of particulate air pollution on blood pressure and heart rate in subjects with cardiovascular disease: a multicenter approach. Environ Health Perspect., 112, 369-77.

Jankovic, J., Jones, W., Burkhart, J, and Noonan, G. (1991). Environmental study of firefighters. Ann. Occup. Hyg., 35, 561-602.

Jones, J., McMullen, M. J., and Dougherty, J. (1987). Toxic Smoke Inhalation: Cyanide Poisoning in Fire Victims. Amr. J. Emerg. Med., 5, 318-321.

Jones, J., and Krohmer, J. (1990). Injury Through Inhalation: Cyanide Poisoning in Fire Victims. J. Emergency Medical Services, 15, 36-39.

Kales, S.N., Soteriades, E.S., Christophi, CA., Christiani, D. C. (2005). Emergency Duties and Deaths from Heart Disease among Firefighters in the United States, New England Journal of Medicine, 356: 1207-15.

Kulis, M.J., Meyer, M.E., Mudgett, P.D., Berger, G.M., and Pilgrim, J.S., Heating of printed circuit board, wire insulation and electronic components for fire signature sensor evaluation, 44th International Conference on Environmental Systems, Tucson, AZ, July 13-17, 2014.

Laden, F., Schwartz, J., Speizer, F.E., Dockery, D.W. (2006). Reduction in Fine Particulate Air Pollution and Mortality. Extended Follow-up of the Harvard Six Cities Study. Am. J. Respir. Crit. Care Med., 173:667–672.

Leonard, S.S., Wang, S., Shi, X., Jordan, B.S. Castranova, V., Dubick, M.A., (2000). Wood smoke particles generate free radical and cause lipid peroxidation, DNA damage, NFκB activation and TNF-α release in macrophages. Toxicology, 150: 147-157.

Levin J.O. et al. (1985). Determination of sub-part-per-million levels of formaldehyde in air using active or passive sampling on 2,4-dinitrophenylhydrazine-coated glass fiber filters and high-performance liquid chromatography. Anal. Chem. 57, 1032-1035.

Lorrain, J.M. Fortune, C.R. Dellinger, B. (1981). Sampling and ion chromatographic determination of formaldehyde and acetaldehyde. Anal. Chem. 53, 1302-1305.

Lowry, W. T., Juarez, L., Petty, C.S., and Roberts, B. (1985). Studies of toxic gas production during actual structural fires in the Dallas Area. J. Forensic Sci., 30, 59-72.

Matsuyama, Y. (2019). Toxic gas and particulates characterization in a smoke density chamber. M.S. Thesis, Case Western Reserve University, May.

Molazemhosseini, A., Magagnin, L., Vena, P., Liu, C.C. (2016). Single-use disposable electrochemical label-free immunosensor for detection of glycated hemoglobin (HbA1c) using differential pulse voltammetry (DPV). *Sensors*, 16 (7), 1024. http://dx.doi.org/10.3390/s16071024

Norris, J.C., Moore, S.J., Hume A.S. (1986). Synergistic lethality induced by the combination of carbon monoxide and cyanide. Toxicology, 40, 121-129.

Peters, A., Dockery, D.W., Muller, J.E., Mittelman, M.A. (2001). Increased particulate air pollution and the triggering of myocardial infarction. Circulation, 103, 2810–2815.

Pope, C.A., and Dockery, D.W. (2006). Health effects of fine particulate air pollution: lines that connect. J. Air Waste Manage. Assoc., 56:709–742.

Pryor, A.J., Johnson, D.E., and Jackson, N.N. (1975). Hazards of smoke and toxic gases produced in urban fires. Combustion Toxicology, 2, 64-112.

Reinhardt, T.E. (1991). Monitoring Firefighter Exposure to Air Toxins at Prescribed Burns of Forest and Range Biomass, Research Paper PNW-RP-441, USDA Forest Service, October.

Reinhardt, T.E., Ottmar, R.D. (2004). Baseline Measurements of Smoke Exposure at Among Wildland Firefighters, Journal of Occupational Environmental Hygiene, 1: 593-606.

Samet, J.M., Rappold, A., Graff, D., Cascio, W.E., Berntsen, J.H., Huang, Y.C., Herbst, M., Bassett, M., Montilla, T., Hazucha, M.J., Bromberg, P.A., Devlin, R.B. (2009). Concentrated ambient ultrafine particle exposure induces cardiac changes in young healthy volunteers. Am. J. Respir. Crit. Care Med., 79, 1034-42.

Seaton, A., Godden, D.W. MacNee, W., Donaldson, K. (1995). Particulate Air Pollution and Acute Health Effects, The Lancet 345, 176-178.

Stefanidou, M., and Athanaselis, S. (2004). Toxicological Aspects of Fire. Vet Human Toxicology, 46, 196-199.

Swann A. (2003). Micro fuel cell fabrication using thick film printing techniques. M.S. thesis, Case Western Reserve University, August.

Takahashi, F., Greenberg, P., Hunter (2014). Firefighter particulate and gas sensor technology, Fire Safety (FS)-World, Fall edition.

Tian, Y. (2019). A study of charring behavior of woods based on internal temperature and CT-scan measurements. M.S. Thesis, Case Western Reserve University, May.

Torén, K., Bergdahl, I.A., Nilsson, T., Järvholm, B.. (2007). Occupational exposure to particulate air pollution and mortality due to ischaemic heart disease and cerebrovascular disease. Occup. Environ. Med., 64, 515-9.

Treitman, R.D., Burgess, W.A., and Gold A. (1980). Air contaminants encountered by firefighters. Am. Ind. Hyg. Assoc. J., 41, 796-802.

Weiss, D.C., Miller, J.T. (2011). A study on chemicals found in the overhaul phase of structure fires using advanced portable air monitoring available for chemical speciation, State of Oregon Governor's Fire Service Policy Council and Tualatin Valley Fire & Rescue, February 25.

Wen, C. (2019). A laboratory scale study of particulates generation from charring and non-charring polymers. M.S. Thesis, Case Western Reserve University, May.

Yeoh, M.J., and Braitberg, G. (2004). Carbon Monoxide and Cyanide Poisoning in Fire Related Deaths in Victoria, Australia. J. Toxicology Clinical Toxicology, 42, 855-863.

Yoshida, M., Adachi, J., Watabiki, T., Tatsuno, Y., and Ishida., N. (1991). A Study on House Fire victims: Age, Carboxyhemoglobin, Hydrogen Cyanide and Hemolysis. Forensic Sciences International, 52, 13-20.

Xu, J.C., Hunter, G.W., Chen, L., Biaggi-Labiosa, A.M., Ward, B.J., Lukco, D., Gonzalez III, J.M., Lampard, P.S., Artale, M.A., and Hampton, C.L. (2012). In Development of High Temperature SiC Based Hydrogen/Hydrocarbon Sensors with Bond Pads for Packaging, Materials Science Forum, Vol. 717-720, pg. 1191, May.